

Master Thesis

Detailed Thermal-Structural Analysis of Fire on a Steel Bridge

A case study comparison of performance-based design against
prescriptive methods

Author: Danny Bond
Student number: 5009170

July, 2024
CIEM0500

Committee Chair: Prof.dr. M.Veljkovic
Main supervisor: Dr. T. Tankova
Second supervisor: Dr.ir. F.P van der Meer
Company: Arup
Company supervisors: Giovanni Milan
Jamie Dennis

Delft University of Technology
Faculty of Civil Engineering and Geosciences

The logo for ARUP, consisting of the word 'ARUP' in a large, bold, serif font.

Preface

This research is about the detailed thermal structural analysis of fire on a steel bridge. Detailed models will be compared against simpler methods used more generally in design. This research project has been done as part of a master thesis for the master track structural engineering in the civil engineering master at the Delft University of Technology. The thesis has been done in collaboration with the company Arup.

This thesis is interesting for anyone with an interest in fire engineering or steel design, and especially for people working in the steel or bridge design industry. Most of the research can be quite well understood by general readers, but some sections do contain some technical terms that require some prior knowledge on structural and fire engineering.

I want to thank Prof.dr. Milan Veljkovic for chairing the thesis committee, Dr. T. Tankova for being my main supervisor and Dr.ir. F.P van der Meer for being my second supervisor. Furthermore, I want to thank Giovanni Milan and Jamie Dennis, my supervisors at Arup, for helping and supporting me within the company.

Amsterdam, July, 2024
Danny Bond

Abstract

The aim of this project is to benchmark the outcomes of a detailed performance based analysis using CFD and LS-DYNA software against codified methods used more generally on projects, and in particular to demonstrate whether this leads to an increase in the predicted capacity of the bridge under fire loading.

The effect and influence of different parameters on the fire resistivity have been investigated. These are the location of the fire, the influence of different live loads, the influence of imperfections, the effect of wind fire interplay, and the effect of internal radiation between surfaces within a structural section.

This research shows that doing a detailed thermal structural analysis of fire on a steel bridge can indeed lead to material savings. Performance based analyses show that the bridge does not fail for the considered fire scenarios for at least 30 minutes. When applying temperatures based on Eurocode, failure is reached after 15 minutes. Using a detailed FEM model to determine critical temperature results in four times less protection necessary than when the conservative Eurocode limit of 350 °C limit is used, a critical temperature of approximately 600 °C is found for the case study.

List of symbols

Latin upper case letters

A_d	Accidental design load	[—]
A_{eff}	Effective cross section area section in CSC 4	[m^2]
A_m/V	Section factor for unprotected steel members	[$1/m$]
E_d	Design effect of actions at normal temperatures	[—]
$E_{fi,d}$	Design effect of actions for the fire situation	[—]
G	Dead load	
N	Normal force	[N]
M_{yy}	Moment around y-y axis	[Nm]
M_{zz}	Moment around z-z axis	[Nm]
P	Pre-stressing load	
Q	Live load	
T	Temperature	[K]
T_p	Temperature of a protective layer	[K]
V	Volume	[m^3]

Latin lower case letters

c_a	Specific heat of steel	[$J/(kgK)$]
c_p	Specific heat of fire protection material	[$J/(kgK)$]
f_y	Yield strength	[N/mm^2]
\dot{h}_{net}	Net heat flux per unit area	[W/m^2]
$k_{E,\theta}$	Reduction factor for the slope of the linear elastic range at the steel temperature θ_a	[—]
k_{sh}	Correction factor for shadow effect	[—]
$k_{y,\theta}$	Reduction factor for the yield strength at the steel temperature θ_a	[—]
t_p	Plate thickness	[m]

Greek upper case letters

Φ	View factor	[—]
--------	-------------	-----

Greek lower case letters

α	Increasing modulus for fire heat release rate	$[kW/s^2]$
α_a	Coefficient of thermal expansion of steel	$[-]$
α_c	Convective heat transfer coefficient	$[W/m^2K]$
ε	Material parameter depending on f_y at normal temperature	$[-]$
ε_f	Emissivity of a flame or opening	$[-]$
ε_m	Surface emissivity of a member	$[-]$
θ	Temperature	$[^\circ C]$
θ_a	Steel temperature	$[^\circ C]$
θ_g	Gas temperature	$[^\circ C]$
θ_m	Element surface temperature	$[^\circ C]$
θ_r	Effective radiant temperature	$[^\circ C]$
λ_a	Thermal conductivity of steel	$[W/(m \cdot K)]$
ρ_a	Steel density (= 7850)	$[kg/m^3]$
σ	Stephan Boltzmann constant] (= $5.67 \cdot 10^{-8}$)	$[W/m^2K^4]$
ψ	Load combination factors	$[-]$

Contents

Preface	i
Abstract	ii
List of symbols	iv
1 Introduction	1
1.1 Research context and problem	1
1.2 Research aim	1
1.3 Research question	1
1.4 Scope and methods	2
1.5 Structure of the report	3
2 State of the art	4
2.1 Fire modeling	4
2.2 Live loads	5
2.3 Wind-fire interplay	6
2.4 Fire resistance	6
2.5 Research gap and position of research	7
3 Conceptual framework	8
4 Research methodology	10
4.1 Research strategy	10
4.2 Case study	11
4.3 The bridge FEM models	12
5 Removed cables	14
6 Prescriptive calculations	19
6.1 Determining steel temperature	20
6.2 Fire protection	22
7 CFD Analysis	26
7.1 CFD input	26
7.2 CFD output	29
8 Thermal analysis	33
8.1 Results for 2.1-meter distance	34
8.2 Results for 3.2 meter distance	35
8.3 Conclusions	37

9 Internal radiation check	40
10 Buckling analysis	44
10.1 Traffic leading	44
10.2 Wind leading	45
10.3 Effect of imperfections	46
11 GMNIA analysis	47
11.1 Bridge capacity with prescriptive thermal load applied	47
11.2 Different fire scenario	53
11.3 Different lateral fire locations	54
11.4 Different longitudinal fire locations	56
11.5 Live load influence	58
11.6 Conclusions	59
12 Comparison of methods	60
12.1 Prescriptive and performance based comparison	60
12.2 Cost and time effectiveness	63
13 Conclusion	65
14 Discussion	67
References	69
Appendix A: Stakeholders and societal impact	73
Appendix B: Thermal material properties	75
Appendix C: Test model	78
Appendix D: Arch and main girder UC calculations	83
Appendix E: Cross section class calculation	86
Appendix F: GMNIA results for different imperfections	87
Appendix G: Increased steel thickness as protection	89

1 Introduction

1.1 Research context and problem

Accidental or deliberate fires on or around bridges can present a risk to the overall strength and stability of a bridge structure. The intense heat from fires can lead to a reduction in the properties of the structural materials, for example reduced Young's modulus and yield strength of steel, or damage to components, which can in turn mean the structure is no longer able to support the applied loading. To protect against this, fire protection measures such as intumescent paints, boarding, or sprayed coatings are applied. However, the application of these measures may often be conservative due to the need to use reasonably simplified, codified methods to allow for the enveloping of many possible fire scenarios. Moreover, most prescriptive fire design is meant for buildings, resulting in assumptions for bridge design being again conservative. This can lead to greater costs, use of materials, and perhaps most importantly environmental impacts.

1.2 Research aim

The aim of this project is to benchmark the outcomes of a detailed performance based analysis using computational fluid dynamics (CFD) and LS-DYNA software against the codified (prescriptive) methods used more generally on projects, and in particular to demonstrate whether this leads to an increase in the predicted capacity of the bridge under fire loading. The research also identifies potential opportunities to improve the balance of complexity, cost, and time, to show if it is actually economical to do such a detailed analysis.

This includes a comparison of; primarily:

- Predicted heating of bridge sections during the fire
- Predicted buckling performance of bridge sections

but also:

- The degree of insight that can be obtained regarding the behavior.
- Level of information required as starting points
- Complexity, cost, and time required to calculate

1.3 Research question

The main research question of this project is: To which extent can detailed modeling of realistic fire scenarios applied on a case study of a 300-meter span steel

arch bridge, bring savings in material use (and carbon emissions) in fire-resistant bridge design, and how can this detailed modeling be made cost and time efficient to be a viable tool for real project design.

Some sub-questions that are related to this research that help answer the main research question and that are discussed in this research are:

- Which locations and components of the bridge need to be assessed?
- What is the effect of taking wind-fire interplay into account?
- Does internal radiation between surfaces within a structural section have a significant effect?
- What is the influence of imperfections and the interaction of those with the heating?
- What is the influence of different live loads on the fire resistivity?

1.4 Scope and methods

A geometrically and materially non-linear model with imperfections (GMNIA) incorporating fire heating has been developed in LS-DYNA by Arup. This model is of steel arch bridge with a span of 300 meter. The model has been used by Arup to predict performance of the bridge for one specific scenario. However, this prediction had numerous limitations, since only one fire scenario was modeled, and influences of fire parameters were not yet fully known. In this research, these different parameter influences are investigated. The existing model will be used and adjusted to perform these investigations.

A 3D CFD analysis done with the software Fire Dynamic Simulator (FDS) is performed to generate input thermal loading for the LS-DYNA model, with potential to address multiple possible fire locations. The LS-DYNA model is used to predict the capacity of the bridge, taking into account the reduction of non-linear material properties from heating (through use of a thermally sensitive material model), structural loading, geometric non-linearities, and initial imperfections based on the expected buckling shape of the plates forming the bridge sections. The buckling modes are pre-calculated using a separate buckling analysis. In parallel, the expected performance under the equivalent load cases is calculated using the methods presented in the Eurocode 1993-1-2 on fire-resistant steel design. The outcomes of the detailed modelling and code based calculations are then compared against the criteria listed in section 1.2. Most of the focus in this research will be on the capacity and protection of the arch. Some analysis on fire located at the cable hangers will be included as well.

1.5 Structure of the report

The structure of this report is as follows: Chapter 2 will give a literary review on the state of the art on the topic of steel bridge fire design. Chapter 3 contains a conceptional framework, depicting how all considered variables in the research relate. In chapter 4, the research methodology is given. Chapter 5 contains the investigation of the cable hangers. Chapter 6 contains calculations on protection from prescriptive methods. Chapter 7, 8, 10 and 11 discuss the whole workflow of the detailed analysis. The CFD analysis is discussed in chapter 7, then the thermal analysis in chapter 8 which also contains the discussion on the effect of wind-fire interplay. The buckling analysis and the sub question on the influence of imperfections is in chapter 10 and the GMNIA including the question on the influence of live loads is discussed in chapter 11. Chapter 9 discusses the sub question on the internal surface radiation, that can be done with the results of the thermal analysis in chapter 8. In chapter 12, the results of the performance based and prescriptive method are compared. Chapter 13 contains the conclusion and chapter 14 a discussion.

2 State of the art

This chapter will show a literary review on different topics that are important for this research.

2.1 Fire modeling

Two different methods are used in the considered literature to take the fire load into account. The first one is a uniform heat increase on a certain surface based on the fire curves from codes. There are a number of standard fire curves in different codes, but all of them are mainly for use in tunnels or buildings and may be not suitable for bridge structures in open-air environments. Little recognized research to bridge fire scenarios definition can be found at present [13]. For bridges, fires can occur due to fuel spillage, these fire types are characterized by intense burning reaching temperatures as high as 900–1000 °C in early stages of the fire [11]. This type of fire is represented by the following fire curve given by equation 1 from Eurocode 1991-1-2 [20].

$$\Theta_g = 1080(1 - 0.325e^{-0.167t} - 0.675e^{-2.5t}) + 20 \quad (1)$$

The other method is a computational fluid dynamics (CFD) simulation to predict the heating of the surface. Fire load curves from Eurocode are not a true representation of an actual fires, and are conservative often[8], doing a CFD simulation may give a better representation, this will most likely have a major effect on the amount of material and protection that is necessary.

In such a CFD simulation, fire can be modeled by specifying the heat release rate (HRR), or the heat release rate per unit area (HRRPUA) of the fire burner as a function of time. By specifying this setting in fire dynamic simulator (FDS), the fire development over time is determined by the manual set burning rate rather than pyrolysis of the burning material by the surrounding environment. So the amount of energy released is fully user defined.

The National Fire Protection Association (NFPA) specifies a range of heat release rates based on different experimental tests for different typical vehicle fires. These are shown in figure 2.1

	Experimental HRR (MW)	Representative HRR (MW)	Time to Peak Representative HRR (min)
Passenger car	5–10	5	10
Multiple passenger cars	10–20	15	20
Bus	25–34	30	15
Heavy goods truck	20–200	150	15
Flammable/Combustible liquid tanker	200–300	300	–

Figure 2.1: HRR values for typical vehicles (figure from [6], values from NFPA 502 (2017))

A commonly defined maximum for the HRRPUA is 2500 kW/m^2 [6].

Within a CFD simulation, fire structure interaction is still a complicated problem with constant interaction between the two. There are two main ways for coupling the fire heat fluxes to the structural model, one is the AST (Adiabatic Surface Temperature) method, the other is the FCHT (Full Conjugate Heat Transfer) method. The first one is a one-way iterative method, the FCHT is a direct coupling form, where solid-thermal analysis models are coupled by CFD and solved together. The first method is most widely used. Results obtained with both the AST method and the FCHT method correspond well with experimental results [28]. The one way coupling (AST method) is often said to be preferred given realistic scale and effort. [7].

The coupling happens by calculating the steel temperatures with results from the CFD, and using those steel temperatures as input for the structural analysis.

Different researchers have compared CFD analysis results to experimental results [7], [27], [28]. All results were in good agreement, making CFD a very suitable tool for obtaining steel temperatures.

2.2 Live loads

Two pieces of research concluded that adding live loads to the bridge does not change the failure type or mode [24] [1]. Only the failure time decreased and the deflections were larger. However, these are cases of relatively short span bridges (12,2 and 37 m), where a uniform live load is applied. No cases were considered of long span bridges and no pattern loading was applied.

2.3 Wind-fire interplay

Wind speed has an effect on the CFD results. Two research efforts conclude that higher wind speeds result in lower peak values of the temperatures [12][25]. However, in both these cases considered the fire was located under the bridge girders, meaning wind will blow the fire away from the considered members. In that case, it is conservative to assume no wind. However, another study [29] that considered fire load on hangers in long span bridges, showed that an increased wind speed did result in increased temperatures. Higher wind speeds result in an increase in flame tilt angle, but in a decrease in area with maximum temperature [13]. This can be seen in figure 2.2. Whether wind needs to be taken into account is thus case study dependent. This latter case corresponds more with the bridge considered in this research, so wind load resulting in wind fire interplay can have a significant effect on the result.

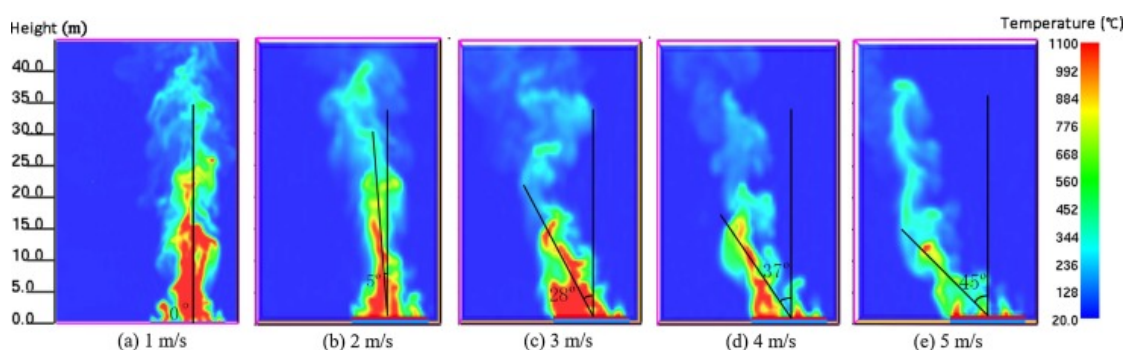


Figure 2.2: Wind-fire interplay (figure from [13])

2.4 Fire resistance

Different studies have been done on the fire resistance of steel members. [2], [10], [9] and [16] all state that the slenderness has impact on the failure/buckling mode. A higher slenderness causes the shear resistance to degrade faster than the moment capacity, because the web temperature increases faster than that of the flanges. The result is that slender beams often fail in shear, and less slender beams, slenderness ≈ 50 , fail in flexure.

A different study [5] investigated the column buckling behavior for different thermal load distributions. It was concluded that different transverse thermal gradients resulted in a significantly different buckling capacity, due to the second order effects developed by bowing due to thermal expansion. An upper bound which resulted in the lowest critical load was found by applying a uniform temperature over the whole cross section. Applying this uniform load is also the usual method

used in Eurocode, which confirms that the Eurocode calculations are conservative.

The study conducted in [17] focuses on the fire resistance of steel beams and columns with the overall imperfection method (OIM). The approach from Eurocode and a GMNIA are also implemented and compared. They conclude that the OIM results are close to the GMNIA results, and that the Eurocode approach is quite conservative. In this research, no fire curves or CFD models were used, but cross-sections had an elevated temperature. This means the Eurocode is not only conservative with the proposed fire loading, but also in calculating the capacity when the same temperatures are used.

2.5 Research gap and position of research

The reports considered in this literary review focus on a number of aspects, all with the goal to make a safer bridge design. One of the important design considerations is which method to use to model the fire (performance based vs prescriptive). The starting point is often no fire resistance measurements, and the insulation is calculated to make the structure withstand the fire for the required amount of time, using either prescriptive methods or performance based methods. In this research the focus lies another way, because it is investigated to which extent material can actually be saved by doing a detailed performance based analysis, and comparing the results against methods in the Eurocode. This will show on which aspects of the fire modeling most savings can be gained.

This research will use the AST method to couple the heat fluxes to the structural model, which is the most commonly used method for coupling. The effect of wind-fire interplay on the steel temperatures will also be investigated in this research, this is something that has been included in some literature, but mostly for analysis on cables only, not on plated steel sections, which is the main focus in this research. Furthermore, in this research, different live loads (load combinations) are applied to see and compare how this affects the buckling and failure mode and the capacity.

3 Conceptual framework

Figure 3.1 shows the conceptual framework for this research problem. The independent variables are depicted in blue, the variables in red are intervening variables that are an intermediate result of the independent variables, necessary to determine the dependent variable. The dependent variable is the required amount of material and fire protection. This is shown in green.

The framework can be read from left to right, starting with applying a fire load. This load depends on the duration of the fire, the location of the fire, whether wind is taken into account, and the model that is used to calculate the fire load. This fire load then affects the material properties of the bridge around the location of the fire.

These material properties, together with the known cross section properties, the applied structural loading and the location of the fire determine the buckling modes of the bridge. The imperfections are set to match the buckling shapes. This buckling load determines the capacity of the bridge. This capacity can then be compared to the loading on the bridge. The comparison between capacity and load leads to the unity check from which it can be determined if extra (or reduced) material and fire protection are needed.

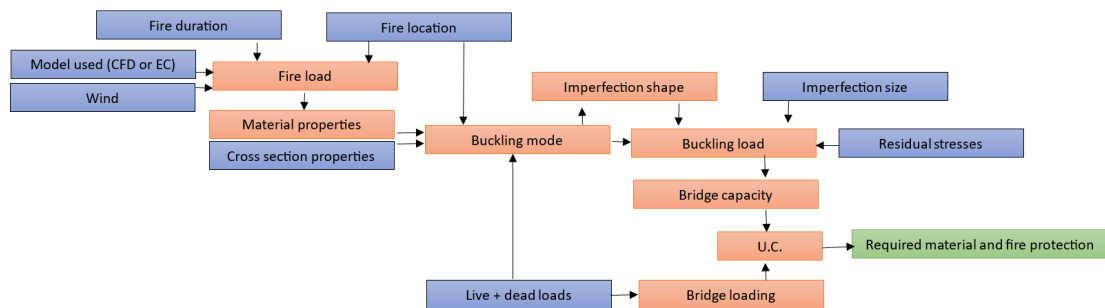


Figure 3.1: Conceptual framework

Some of the independent variables are determined for this project, these are the material properties and cross section properties and the dead load of the bridge. The rest of the independent variables can be altered and will affect the outcome as well. These are: The model that is used for the fire load, the wind speed, the location of the fire, the duration of the fire and the live load on the bridge. The size of the imperfection can also be varied, but can also be taken as the maximum tolerance value specified in codes.

[14] states that there are studies saying the effect of residual stresses is negligible for the member stability at elevated temperatures, but that there is also one study [4] that did observe a 15 % reduction in lateral torsional buckling resistance. The influence of these stresses will not be investigated in this research. For the structure type considered, lateral torsional buckling is not a relevant failure mode. Eurocode 1993-1-14 also states that the residual stresses do not have to be considered since they are negligible in fire situations [26]. But in general, it is important to know if they are taken into account or not.

4 Research methodology

4.1 Research strategy

An existing LS-DYNA model of a steel arch bridge is used to predict performance under fire loading. LS-DYNA is an advanced Finite Element Method (FEM) software in which nonlinear and multi-physics problems can be modelled. This makes it a suitable software to model a geometrically and materially non-linear analysis with imperfections, subjected to fire heating. The model of the bridge in LS-DYNA can be seen in figure 4.1

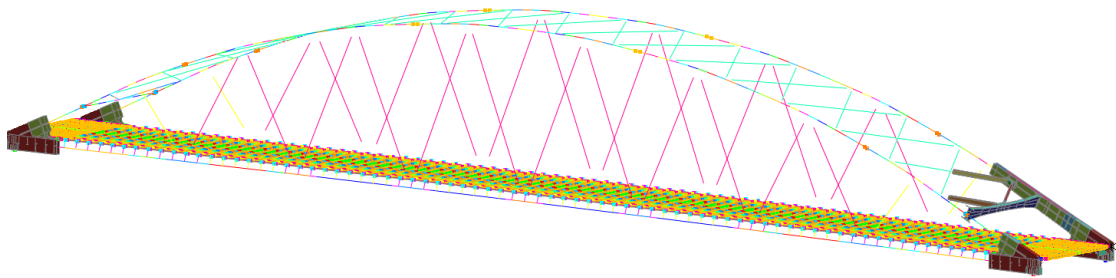


Figure 4.1: FEM model of the bridge

The fire loading needs to be applied to see how temperatures in the material change. For this, CFD simulations are used. Wind is taken into account here, to be able to investigate the wind-fire interplay, this has effect on the spreading of the fire. The CFD simulation is done with the software Fire Dynamic Simulator (FDS).

The FDS output consist of radiation and convection data for specified points around the fire. This is produced for different cases, where both an open truck fire and a closed truck fire are considered for 2 different wind speeds. This input is then modeled for different lateral and longitudinal positions of the (truck) fire. The convection and radiation are then used as boundary condition in a thermal model to calculate the temperature of the steel over time.

The material properties can then be reduces with their reduction factors based on the resulting temperature.

A separate linear buckling analysis is then done to determine the buckling modes and shapes. Live loads need to be applied in this analysis. The buckling modes from this analysis are the input shapes of the geometrical imperfection that are

added to the model. With these imperfections included, a fully nonlinear analysis can be performed to determine the performance of the bridge.

The linear buckling analysis is completed for 2 different load cases. One with wind leading and one with traffic leading. These load cases are determined with the accidental load combination formulas from Eurocode given in equation 2

$$E_d = \sum_{j \geq 1} G_{k,j} + ' P' + ' A'_d + \psi_{1,1} \cdot Q_{l,1} + \sum_{i > 1} Q_{k,i} \quad (2)$$

A full GMNIA analysis will then be completed for the different combinations of fire scenarios and load cases. For each of these analyses, the resulting capacity of the structure is then determined with the FEM results. It is expected that certain situations and fire scenarios are governing over others. Therefore, a GMNIA analysis will not be done for every possible fire scenario and load combination. Based on the thermal analysis results, possible critical fire scenarios are identified and those are considered in the GMNIA analysis.

In parallel, the expected performance under the equivalent load cases are calculated using methods presented in the Eurocodes. The Eurocode methods that will be used are protection calculations based on a critical steel temperature, and the capacity of the model, with uniform temperatures applied on the model, based on temperature curves from the code. So in total 3 methods will be compared.

1. Necessary protection based on critical temperature prescribed by code
2. Capacity and protection based on code based temperature applied on the FEM model
3. Capacity and protection based on detailed performance based analysis

The outcomes of the different methods are then compared on the following points:

- Predicted heating of bridge sections during the fire
- Predicted buckling performance of bridge sections
- The degree of insight that can be obtained regarding the behavior
- Level of information required as starting points
- Complexity, cost, and time required to calculate

After that, possible material savings can then be determined and calculated.

4.2 Case study

For this thesis, a model of a real existing bridge is used. The main research question is: To which extent can detailed modeling of realistic fire scenarios applied on

a case study of a 300-meter span steel arch bridge, bring savings in material use (and carbon emissions) in fire-resistant bridge design, and how can this detailed modeling be made cost and time efficient to be a viable tool for real project design. It is necessary to investigate the response to fire loading on a realistic bridge. It is therefore logical to apply this on a real structure, so the acquired knowledge can be used for real life assessment as well at the end of the research. A stakeholder and societal impact analysis for this case study and research in general is given in Appendix A.

The bridge that is considered is a 300-meter span steel arch bridge. The project details will not be identified for confidentiality reasons.

4.3 The bridge FEM models

For the complete analysis, 3 different type of models have been made, each with different loads, material properties and boundary conditions. These 3 model types are the thermal model, the buckling model and the GMNIA model.

For the thermal analysis, only the parts subjected to thermal loading are modeled, which are only the parts modeled as shells in figure 4.1. No structural loads are applied yet. The boundary conditions in the thermal model are radiation and convection. Because the required times of fire resistance are relatively high compared to normal analysis, the thermal analysis makes use of a thermal speed up factor (TSF). This TSF speeds up the temperature distribution, while the structural response follows the time in the analysis. For all thermal analysis, the TSF has been set to 1000, meaning 1000 seconds of temperature development happens in 1 second in the analysis. This way, 30 minutes of fire is 1.8 s in the analysis. Making the time to run the analyses significantly shorter.

For the buckling analysis, the dead and different live load combinations are included. The thermal materials are modeled with shells the same way as in the thermal analysis, but the rest of the structure is now modeled as well with beam elements. For the buckling analysis, no thermal boundary conditions are applied, the only boundary conditions are 4 single point constraints at 4 nodes where the degrees of freedom can be specified. These nodes are fully constraint, and are connected through a spring support to another node, which in turn is coupled rigidly to the bridge support. The spring supports have translational stiffnesses and constraint, but no rotational stiffness. In essence this means that the bridge is on hinge supports, which have the possibility to translate to some extent but with very high stiffness. These same support boundaries are used in the GMNIA model.

For the GMNIA analysis, all shells are modelled with a material type where the properties depend on the temperature. The temperature dependent properties can be set as required. In the model, the following properties are temperature dependent: Youngs modulus, yield stress, the coefficient of thermal expansion, the specific heat and the thermal conductivity. These material properties are specified according to NEN-EN 1993-1-2 and the values are given in Appendix B.

In the GMNIA models, gravity and live loads are first applied gradually with a large amount of global damping in the model to exclude dynamic effects. Then the damping is removed and the thermal load profile, which is the result of the thermal analysis, is applied.

The entire analysis consists of a series of complex steps. To make sure each step is done correctly, the steps have first been applied on a small scale test model. With this test model, it could be checked if correct results are obtained in each analysis, and sub steps could be validated, before doing the steps with the model of the whole bridge. The test model and its results are given in Appendix C.

5 Removed cables

The main focus of the assessment in this research is on the arch and arch springing point, but there is also the possibility that the fire occurs at the location of the hangers. To take this into account, an analysis has been done, where it is assumed that 2 of the cables connected to the same hanger fail at a certain moment due to the presence of a fire there. No detailed thermal or GMNIA analysis are done at the cables to see the response, they are just assumed to fail when a fire is present. Hangers at the deck level, which are not connected at the same location, are at least 27 meters apart. It is therefore not necessary to check simultaneous failure of cables from two different hanger connections on the deck. 4 different sets of 2 cables failing are checked numbered from 1 to 8 from left to right, these are shown in figure 5.1. it is assumed that other locations behave the same because of symmetry.

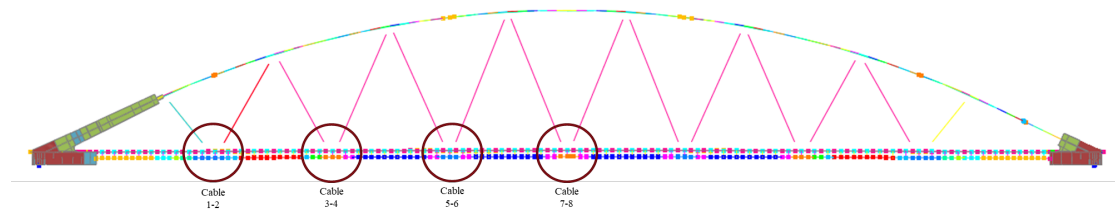


Figure 5.1: Locations of hanger losses considered

In the model, first the dead load (gravity) is applied, then the live loads. Both with a high amount of global damping present to prevent any dynamic effect being presents after applying the loads. After that, the global damping is removed, and 2 cables are removed from the construction. Dynamic effects are then taken into account.

Since the cables are modeled as an elastic material, it needs to be checked for each of the remaining cables if the forces remain positive (Cables can only take tension, no compression) and if the forces remain below the Ultimate Limit State (ULS). The ULS strength for the cables is 10974 kN, except for the outer ones, for which it is 12648 kN. For this ULS force, the cables are still in the elastic region, which makes modeling it as an elastic material very suitable. The arch springing points are checked for plastic strains and Von Mises stresses as well, and a part of the arch, which is modeled with shells, can also be checked. Since the hangers take vertical forces from the deck to the arch, it is expected that the traffic leading load combination is governing.

Figure 5.2 show the forces of all hangers except the 2 removed ones vs time. It can

be seen that all forces remain positive and that the forces are all below the 10974 kN, since the maximum force is 10359 kN. It can also be seen that the forces first increase from 0 to 2 seconds, this is where the gravity load and later live loads are applied, and are then (approximately) constant for a second before the cables are removed, after which the forces vary dynamically. This confirms the cables behave correctly and according to the model input. This output is for the traffic leading load combination, for the wind leading the maximum force was 9146 KN, and the forces in the cables before cable removal are higher as well for all cables, so traffic is clearly governing. The other hanger loss analyses are thus only done for the traffic leading combination.

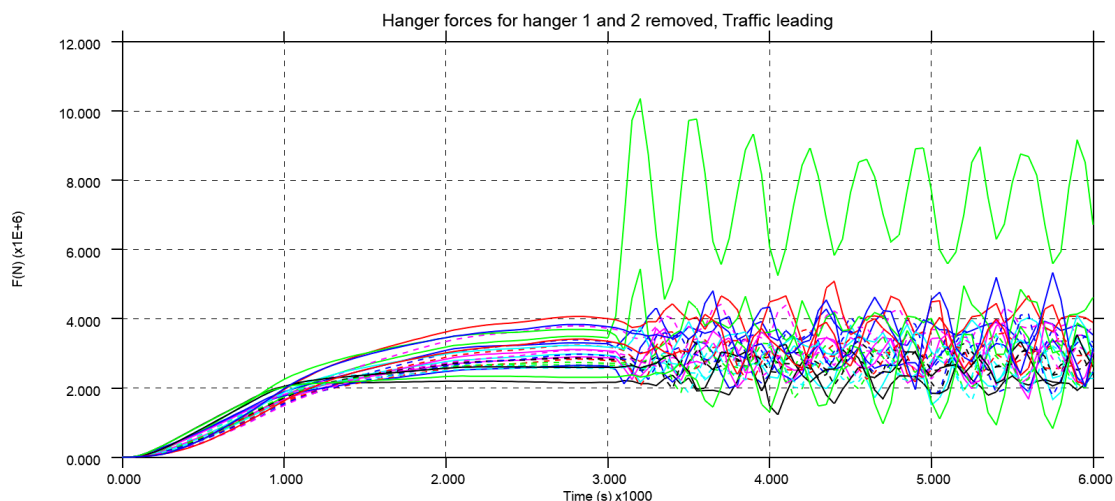


Figure 5.2: Hanger forces vs time

For the cables, no prestressing forces are included. The actual design of the bridge does not require prestressing of the cables, since the minimum tension forces in the hangers are always reached. However, the code [22] does specify that an increase in force of 10% of the self weight and permanent loads needs to be taken into account. The hanger capacity will still be sufficient when this is included. However, this is not included in this analysis and figure.

For hanger loss 1 and 2: Some plastic strains occur in the arch springing points and arch. However, the plastic strain that is occurring is very local and only 6.4% of the failure strain. Stresses can easily redistribute around this region. So cables and arch springing point have sufficient capacity for these hangers to be lost.

For all other hanger loss cases, no plastic strains occur in the arch springing point, and the maximum hanger forces are lower for these scenarios. Table 1 shows the

Table 1: Hanger forces and unity check for different hanger loss scenarios

Hangers lost	Max hanger force (kN)	UC
1 & 2	10359	0.94
3 & 4	8919	0.81
5 & 6	8478	0.77
7 & 8	8213	0.75

maximum hanger forces and the unity check for the different hanger loss scenarios. For all scenarios, the hangers and arch springing point have sufficient capacity. So far, this is only a verification of the strength of the cables and the arch springing points. Extra calculations and unity checks still need to be done on each section of the main girder (MG) and the arch before conclusions can be made on whether fire protection is necessary for the cable hangers and hanger connections.

For this removed cable analysis, numerous sections of the arch and main girder have been checked. The sections that have been checked are the sections that seem to be critical based on the absolute maximum bending moments and forces over time. An example of this for hanger loss 1 and 2 can be seen in figure 5.3. If this will be used in actual design, all section of the arch and main girder need to be checked, since the properties of the sections differ along the length.

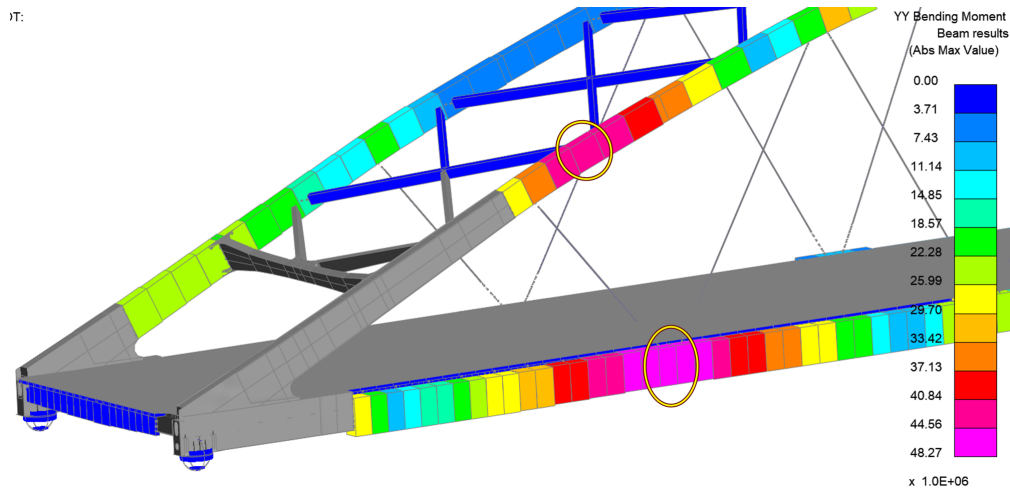


Figure 5.3: Absolute maximum bending moment and locations considered to be critical for hanger loss 1 and 2

In total, 4 arch and 6 main girder elements have been checked for the 4 different hanger loss combinations. The arch and main girder sections are checked for

strength according to NEN-EN1993-1-1 [21] and NEN-EN1993-1-5 [23] for bending and axial forces, using the rules for cross-sections in CSC 4 accordingly.

The resulting unity checks can be seen in table 2. A more detailed explanation and the calculation sheet for these Unity Checks are given in Appendix D.

Table 2: Unity Checks arch and main girder sections

Section	x-position (m)	UC
Hanger loss 1-2		
Arch (B16)	44	0.74
MG (10028)	49	1.20
Hanger loss 3-4		
Arch (B14)	39	0.64
MG (B10047)	84	1.17
MG (B10065)	116	1.08
Hanger loss 5-6		
Arch (B42)	116	0.76
MG (B10063)	112	1.10
Hanger loss 7-8		
Arch (B54)	150	0.76
MG (B10083)	150	1.31
MG (B10101)	183	1.11

The unity checks show that the arch sections are able to resist the loads resulting from hanger loss, but the main girder is not. However, there is a potential in considering the hangers in more detail. In the current analysis, there are still some limitations that result in different forces and moments.

Limitations of the model.

- Load stages are taken into account in the model. However, actual construction stages of the bridge are not. The whole bridge is so called wished in place, which can result in different (usually higher) forces and moments
- Cables are fully removed in an instant, this results in large dynamic effect. In case of an actual fire, the stiffness and strength of the cables will first gradually reduce before they snap, resulting in less dynamic effect than in the model used here.
- For the unity checks, the maximum (or minimum) forces and moments have been used that have occurred during the analysis. It is possible that maximum bending moment around one axis does not occur at the time as the

maximum bending moment around the other axis and the maximal normal force. Therefore, this is a conservative assumption.

From this analysis, it can be concluded that the hangers itself cannot be left unprotected. A fire scenario where 2 hangers of the same hanger connection fail results in insufficient capacity for the rest of the bridge. However, in a more detailed analysis, this conclusion might be different. A detailed analysis could show that the cables do not fail at all in certain fire scenarios, that the critical temperature is higher than the 300 °C limit currently used in the design, or that the bridge still has enough capacity when modelled in more detail (shells instead of beams) and without the current limitations.

6 Prescriptive calculations

The Eurocode contains rules and guidelines regarding fire safety design. However, most of these guidelines are based on fire design in buildings. Little to no information is given for bridge fires specifically. For designing cross-sections in cross section class (CSC) 4, like the arch and ASP sections, there are different general ways to design for fires. One method is to determine the critical temperature (critical $k_{y,\theta}$ value) for which the cross section still has a Unity Check (UC) < 1 based on a detailed cross section analysis, this is a calculation in temperature domain, the forces in the members are taken into account here. Based on that critical temperature, it can be determined how much fire protection needs to be applied to make sure this is not reached after 30 minutes, this is the time the bridge needs to be able to withstand the fire before help arrives. However, forces due to thermal expansion need to be taken into account here, these are difficult to determine for such a complicated structure. Therefore, this option will not be explored.

The other method is directly calculating the amount of the fire protection needed, based on a critical steel temperature of 350 °C (for CSC 4), as specified in NEN-EN 1993-1-2 section 4.2.3.6. This method is a calculation in temperature domain (but with the resulting critical temperature already given). The required duration of the fire is 30 minutes. No forces are taken into account in this method.

Appendix E shows the calculation of the cross section class for the first section of the arch at the location of the arch springing point (ASP), which location is shown in figure 6.1a and its cross section in figure 6.1b, The is CSC 4.

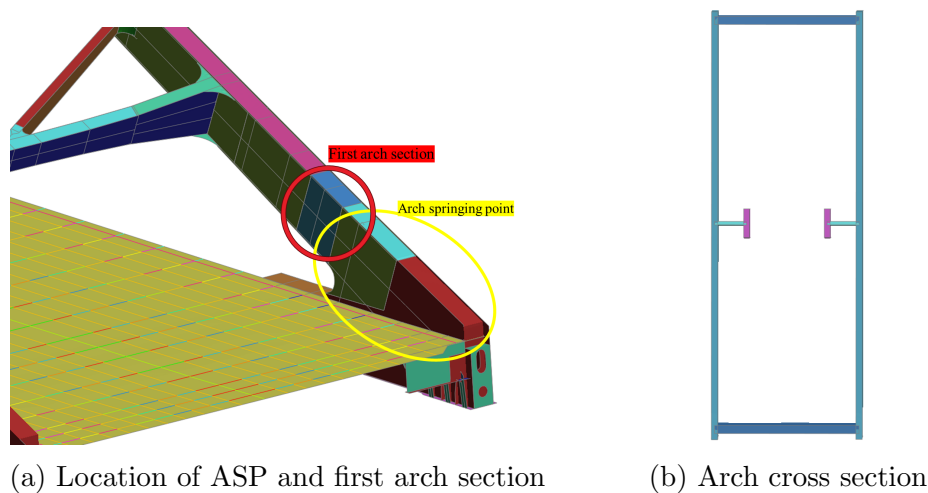


Figure 6.1

6.1 Determining steel temperature

The temperatures of the steel can be determined based on the temperature of the air at the steel surface, and the energy radiated from the fire onto the steel surface. When prescriptive methods are used, bridge fires are characterized by the hydrocarbon fire curve, for which the gas temperature is given by equation 3.

$$\Theta_g = 1080(1 - 0.325e^{-0.167t} - 0.675e^{-2.5t}) + 20 \quad (3)$$

The steel temperature can be determined with equation 4.25 from NEN-EN 1993-1-2

$$\Delta\theta_{a,t} = k_{sh} \frac{A_m/V}{c_a \rho_a} \dot{h}_{net,d} \Delta t \quad (4)$$

A_m/V is the section factor, this depends on the area which is exposed to fire and the element volume, for a 3 sided exposure of a web or flange, this factor is approximately equal to $1/t_p$ (for thin walled sections). For 4 sided exposure, this value is $2/t_p$, which is twice as much. Figure 6.2 illustrates what the different exposures would look like.

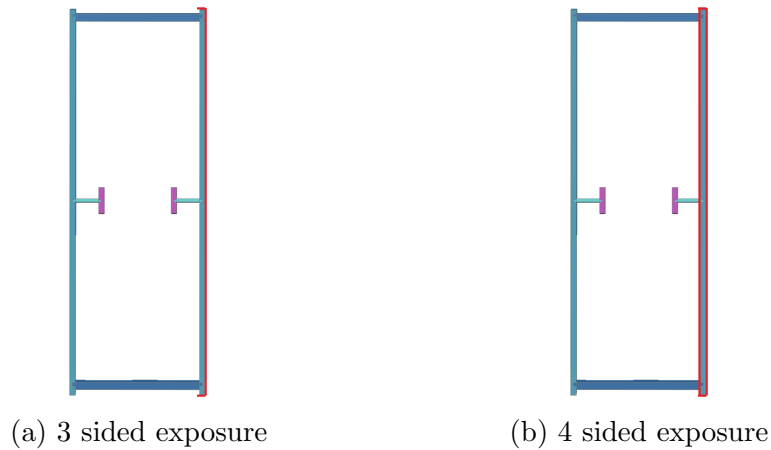


Figure 6.2: Different possibilities for section faces exposed to fire

The situation considers a rectangular hollow section. So the inside of the web is not directly exposed to the fire. Therefore, it is chosen to take A_m/V for 3 sided exposure.

$\dot{h}_{net,d}$ is the design value of the net heat flux per unit area given by:

$$\dot{h}_{net} = \dot{h}_{net,c} + \dot{h}_{net,r} \quad (5)$$

$$\dot{h}_{net,c} = \alpha_c(\Theta_g - \Theta_m) \quad (6)$$

$$\dot{h}_{net,r} = \Phi \cdot \epsilon_m \cdot \epsilon_f \cdot \sigma[(\Theta_r + 273)^4 - (\Theta_m + 273)^4] \quad (7)$$

For elements surrounded by the fire, the gas temperature Θ_g be set equal to the effective radiant temperature Θ_r .

$$\alpha_c = 50 \text{ W/m}^2\text{K} \text{ (As specified by EC)}$$

$$\varepsilon_f = 1.0$$

$$\varepsilon_m = 0.8 \text{ (As specified by EC)}$$

$$\sigma = 5.67 \cdot 10^{-8} \text{ W/m}^2\text{K}^4$$

$\Phi = 1$, this is the view factor, assuming a view factor of 1 is conservative, this would mean the fire is fully covering (touching) the web (all the web can see is fire)

With these equations, and the known air and gas temperature taken as specified in equation 3, the temperature of the steel can be calculated. The thickness of the sections vary along different parts of the arch, the arch springing point and the portal. Therefore, different A_m/V factors occur, resulting in different steel temperatures for the different sections over time. The result can be seen in figure 6.3

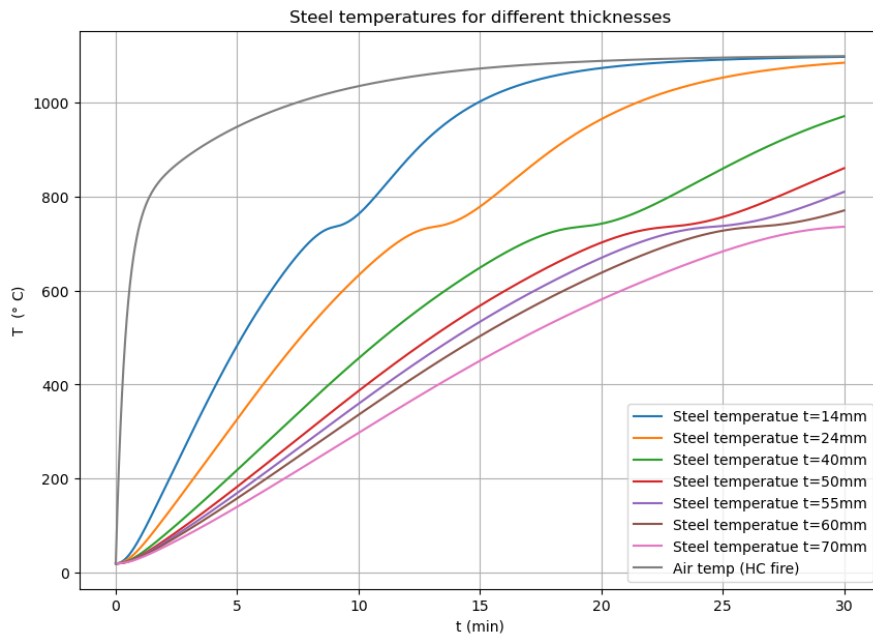


Figure 6.3: Steel temperature for different section thicknesses from hydrocarbon (HC) fire

These steel temperatures over time are used as input to further analysis with the FEM model.

6.2 Fire protection

For the protective layer, intumescent paint can be used, this is a paint that reacts and expands once it reaches a certain temperature level, creating an insulation layer around the steel. For the calculations of the steel temperatures, an equation has been used from [3]. In Eurocode NEN-EN 1993-1-2 equation 4.27, the code assumes that the temperature of the coating is the average of the fire and the steel temperature. However, the thermal conductivity is highly dependent on the temperature and the rate of heating of the coating. Therefore, it is necessary to calculate the temperature of the coating more accurately. That is why the equation from [3] is used, where the radiation on the coating **surface** is included as well, and the coating temperature is calculated as the average temperature of the surface of the coating and the steel temperature.

$$\Delta T_a = \frac{A_p/V}{(1/h + \frac{d_p}{\lambda_p})c_a\rho_a} \frac{(T_g - T_a)}{(1 + \phi/3)} \Delta t - (e^{\phi/10} - 1)\Delta T_g \quad (8)$$

Where:

$$h = (T_g^2 + T_a^2) \cdot (T_g + T_a) \quad (9)$$

$$\phi = \frac{c_p\rho_p d_p A_p/V}{c_a\rho_a} \quad (10)$$

In this equation, it is important to take have temperatures is Kelvin, since the radiative flux is calculated within the equation.

The density and specific heat for protective layers may be taken as:

$$\rho_p = 100 [kg/m^3]$$

$$c_p = 1000 [kJ/(kgK)]$$

The real values of these parameters for intumescent paints can be higher than this. However, the influence of these values is investigated by changing the order of magnitude and observing the change in results. The effect is very small, and using higher values results in a decrease of the maximum temperature. So taking these values is conservative. Because of the negligible effect on the outcome when changing these parameters, these standard Eurocode values are adopted.

The thermal conductivity of the protective layer (λ_p), is influencing the resulting steel temperatures significantly. This is why a more precise temperature of the coating is calculated. The surface temperature of the coating is calculated with equation 11.

$$T_{surface} = T_g - \frac{T_g - T_a}{1/h + d_p/\lambda_p} / h \quad (11)$$

The temperature of the coating layer is then taken as:

$$T_p = \frac{T_{surface} + T_a}{2} \quad (12)$$

And the rate of the heating of the coating:

$$\Delta T_p = \frac{T_{p(t+\Delta t)} + T_{p(t)}}{\Delta t} \quad (13)$$

Based on these 2 parameters from equation 12 and 13, the thermal conductivity of the intumescent paint can be determined with figure 6.4

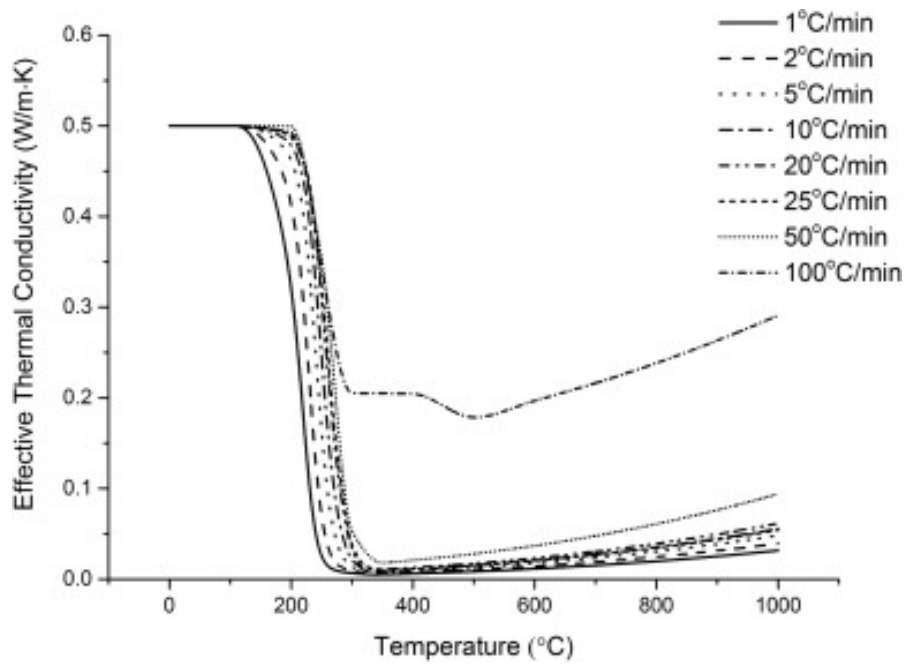


Figure 6.4: Thermal conductivity of intumescent coatings ([3])

This thermal conductivity can then be used in equation 8. The thickness of the protective layer can now be tuned based on the critical temperature for the cross section.

For a critical steel temperature of 350 °C. Which is the limit that can may be taken for CSC 4 sections, the required thicknesses of the protective layer for different steel section thicknesses is given in table 3

Table 3: Required protection thicknesses

Section thickness (mm)	Protective layer thickness (mm)	Section Area (m^2)
40	3.6	16.2
50	2.7	20.2
55	2.4	31.53
60	2.1	18.66
70	1.7	7.56

Figure 6.5 shows the thicknesses of the steel in m used in the design.

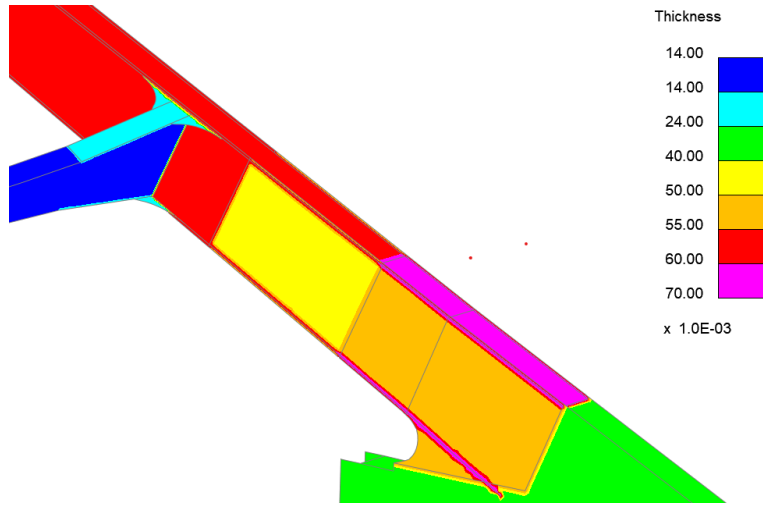


Figure 6.5: Section thicknesses at the arch springing point

The sections areas are also shown in table 3. These areas only include the bottom flange and inner web of the arch up until portal height. The total protection volume for each ASP = $0.24 m^3 = 240.06 L$, applying this on 4 sides results in 962.3 L of intumescent paint.

For an intumescent paint that can be used in an outside environment (Firetex M90/02 at Sherwin Williams), the price is 2450 euro per 60 kg (L), which means at least 39200 Euro of paint is necessary (likely more to have a margin for inaccuracy, spillage and safety factor). When protection all around the arch springing point is chosen, the price will approximately double.

It is important to note that the data of thermal conductivity is from a different source than the supplier of the intumescent paint. The properties for this specific paint may differ to some extent. It is therefore important to do a more

detailed investigation into the properties or discussion with the supplier before applying certain thicknesses of the paint. Calculations are just to give an indication of the minimum costs for the paint product only and do not consider costs of labor, coordination, or other costs incurred in actually applying the paint. These calculations are only based on the 350 °C limit from Eurocode, and do not consider any models yet.

7 CFD Analysis

This chapter describes the computational fluid dynamics analysis, which is performed to obtain the thermal boundary conditions for the performance based analysis.

7.1 CFD input

The computational fluid dynamics (CFD) simulations have been performed with Fire Dynamics Simulator (FDS). This used a large eddy simulation code, which is a mathematical model for simulating turbulence, so heat transport of fires can be modeled. The fire specifications have to be modeled or specified in an FDS input text file.

The critical design fire scenario is a 16-meter-long heavy good vehicle. The fire intensity can be specified in FDS by setting the maximum heat release rate per unit area. For this project, the HRR has an ultra-fast growth rate. The shape of the HRR rate vs time can be seen in figure 7.1. After the maximum is reached, the HRR is kept constant up to the end of the simulation. For confidential reasons, the values are not given in this report.

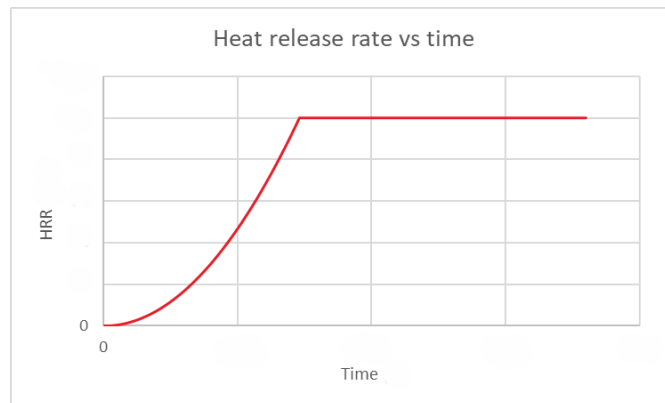


Figure 7.1: Heat release rate vs time

The domain in which the fire is modeled has dimensions (x,y,z) $57.2 \text{ m} \times 38.4 \text{ m} \times 21.6 \text{ m}$. The mesh is divided in different sub-meshes so that it can be run on different processors. Figure 7.2 shows an overview of the different meshes in the XY plane. The cells in the mesh all have a size of $0.2 \text{ m} \times 0.2 \text{ m} \times 0.2 \text{ m}$, except for the wind mesh, which has a size of $0.4 \text{ m} \times 0.4 \text{ m} \times 0.4 \text{ m}$.

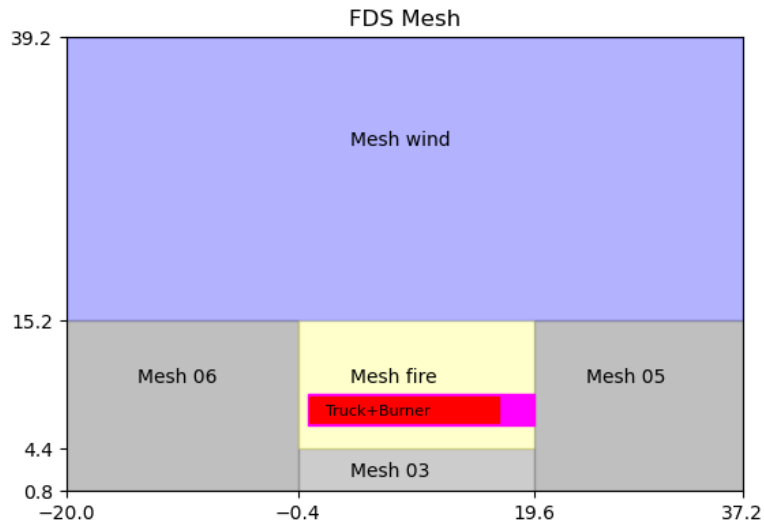


Figure 7.2: Mesh domains used in FDS

For the initial conditions, FDS assumes an ambient temperature of 20 °C everywhere. By default, FDS assumed solid boundaries outside the meshed domain. Therefore, manual boundary conditions have been applied on 3 sides (Xmin, Xmax, Ymin) and on top (Zmax) of the domain called 'OPEN', which specify that the ambient temperature of 20 °C continues outside this domain. The wind that is taken into account must be specified in FDS as well. In the simulation, the wind speed is taken as constant, and the wind is already present before the start of the fire, to make sure the wind speed is in a steady state. This wind is the boundary condition applied on the remaining side (Ymax), the wind is applied as a constant value, and it is blowing towards the bridge.

An FDS file was already created by Arup for one scenario where there was a truck with an open roof and a wind speed of 3 m/s was present. The geometry of such an open roof truck fire can be seen in figure 7.3.

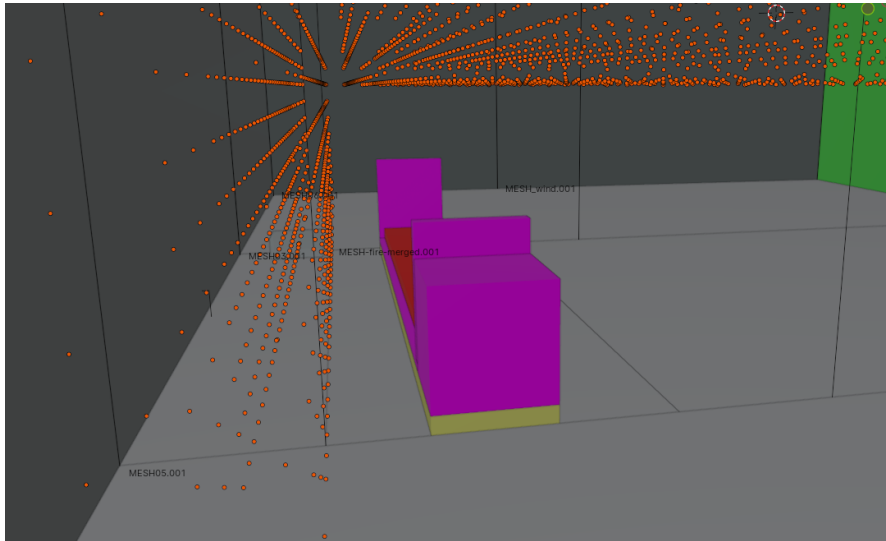


Figure 7.3: Obstruction geometry of the FDS file and data points

For this research, both open truck fires and closed truck fires are considered. To make a closed truck, the extra roof geometry needs to be modelled, this has been done by adding so called 'obstructions' into the FDS file. The result is shown in figure 7.4 In both the open and closed roof scenario, the sides of the truck are open.

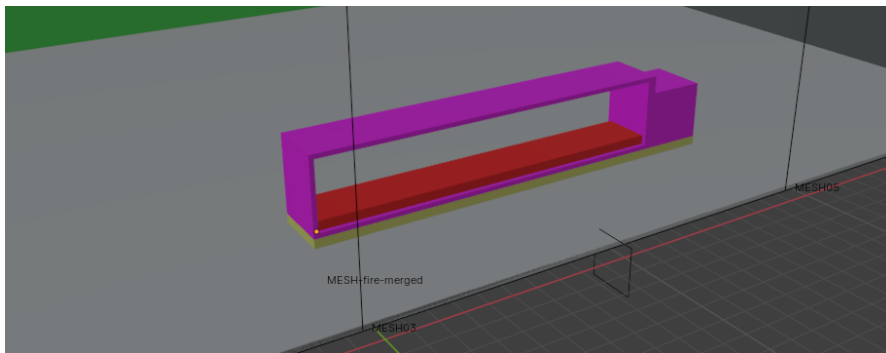


Figure 7.4: Closed truck geometry as modelled in FDS

4 different FDS files have been created. These 4 different files have the following differences.:

- Open roof truck with a wind speed of 3 m/s
- Open roof truck with a wind speed of 2 m/s
- Closed roof truck with a wind speed of 2 m/s

- Closed roof truck with a wind speed of 5 m/s

These values for the wind speed were chosen based on simulations that were already performed by Arup where only air temperatures were computed, (so radiation not yet accounted for). These air temperatures depend on the locations of the flames of the fire and the radiative flux will likely be affected by that as well. A closed truck fire with 5 meter per second wind speed resulted in the highest temperatures at low heights (close to the deck), and could thus be critical for the arch springing point. The lower wind speeds result in the flame going higher and affecting higher zones of the arch. The 4 cases that have been chosen all have a potential to be critical.

The FDS files specify many points around the fire for which data is output. In this case, it is the temperature and the radiative heat flux that is calculated for each of those data points. The coordinates are chosen such that they are close to the arch, the ASP and the portal, which are the locations of interest of the bridge.

The bridge geometry is not modeled in the FDS domain to allow the CFD domain to be translated relative to the bridge model in one direction. This might influence the resulting temperature and radiation data of the measurement points. This is a known limitation, but will not be further considered.

7.2 CFD output

The location of the fire is fixed with respect to the CFD data points. So, to model the location of the fire w.r.t the bridge, the bridge has to be moved to the correct locations w.r.t. the CFD data points. The truck fire has a length of 16m. Two different longitudinal fire locations are considered which are shown in figure 7.5, the different fire locations are spaced 4 meters apart. Location 1 affects the arch springing point more, and location 2 extends to under the portal. Figures 7.5 and 7.6 also show the locations of the data points w.r.t the bridge.

For the lateral position of the truck, 2 different options have been considered as well. In one scenario, the distance from the edge of the truck to the arch is 2.1 m, This is chosen since this is the most critical realistic scenario, because the truck cannot get closer than that due to the presence of railings. In the other scenario, this distance is 3.2 meters. This way, the influence of the lateral position on the steel temperatures can be investigated as well.

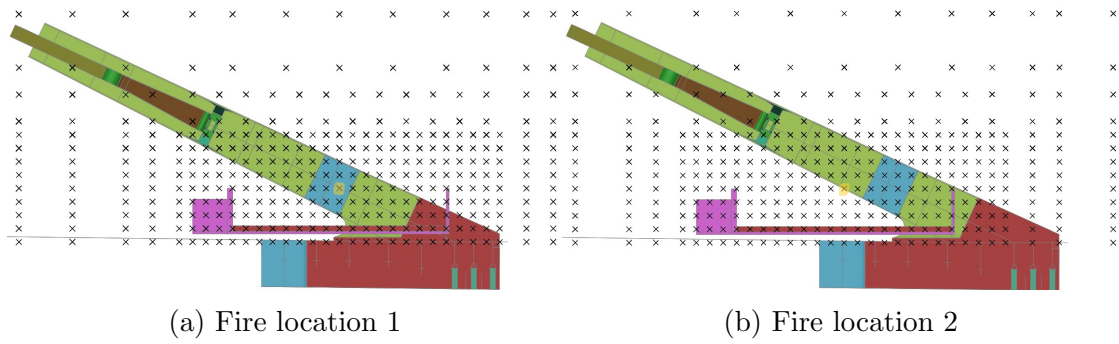


Figure 7.5: Fire locations and CFD data points

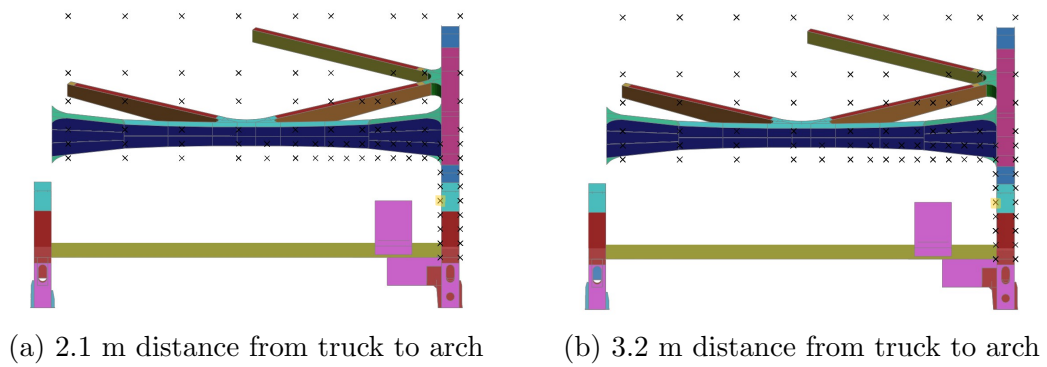


Figure 7.6: Lateral fire locations and CFD data points

The results of the CFD simulation are Temperatures ($^{\circ}\text{C}$) and radiative heat fluxes (kW/m^2). An example of the CFD results for one of the data point on the bridge surface close to the fire (point that is highlighted in figures 7.5 and 7.6) can be seen in figure 7.7.

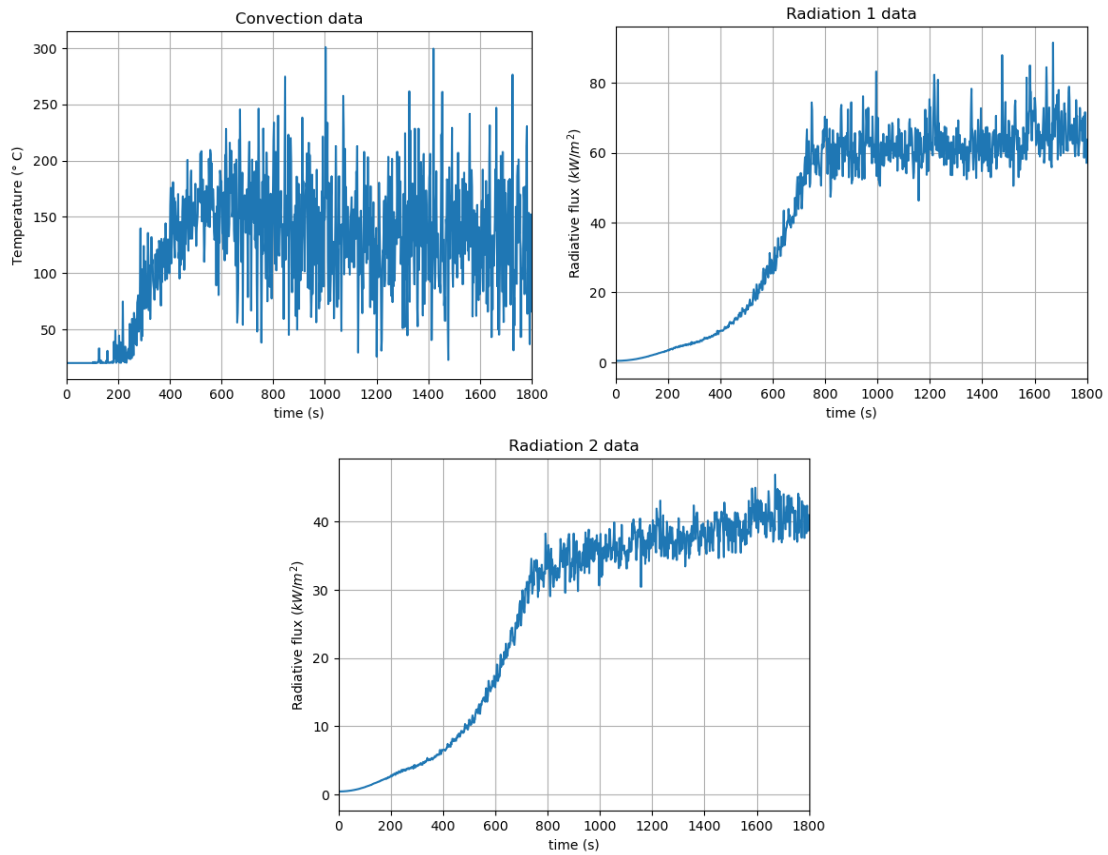


Figure 7.7: CFD results for 1 data point

Two different heat fluxes are computed for every data point. This is done to take the orientation of the steel surfaces into account. The outer web of the arch and the ASP have a different angle towards the fire than the bottom flanges. These orientations of every element have been specified before running the analysis. The distance and orientation of the faces is thus taken into account explicitly. Convection is applied on all shells, Radiation 1 is applied on all shells of webs facing the fire and Radiation 2 is applied on all shells of flanges facing the fire, these different shell sets are highlighted in figure 7.8

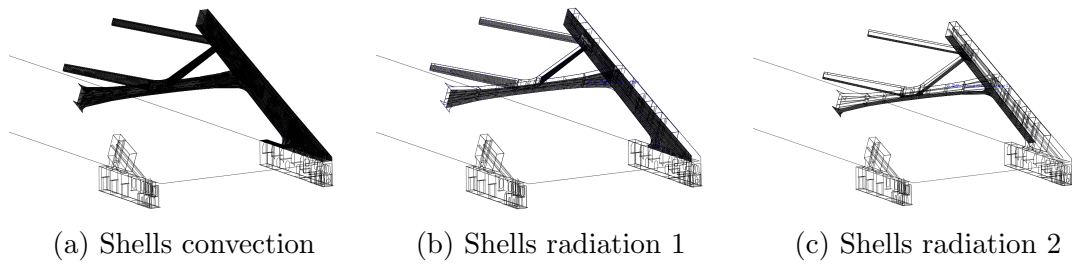
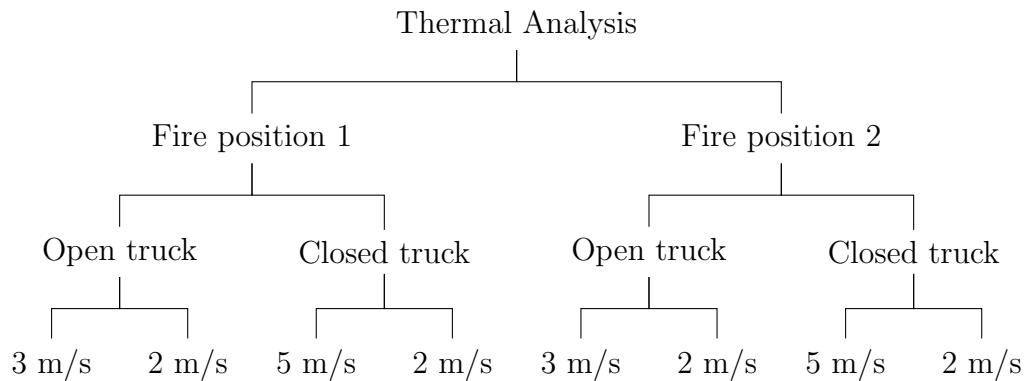


Figure 7.8: Shell sets on which the different CFD results are applied

8 Thermal analysis

For the thermal analysis, the resulting temperatures and radiative heat fluxes obtained from the CFD runs need to be converted to convection and radiation boundary conditions on the thermal model. For this, JavaScript routines have been adopted to automate the mapping between FDS and LS-DYNA. Different thermal analysis have been performed for the different fire locations, scenarios and wind speeds. This is shown in the overview below.



These different scenarios are considered for 2 different lateral distances from the edge of the truck to the face of the arch. This lateral location is taken into account in the CFD results. A distance of 2.1 m and 3.2 meter from truck to arch are considered. This leads to a total of 16 different thermal analysis.

Two different models were made where the location of the bridge was different. The fire location is fixed (has fixed coordinates in the CFD), so to change the fire position, the bridge was moved with respect to the fire. For each of these models, the different CFD results were used.

The scripts were run on a programming interface within the model in Oasys primer, which is a pre-processor of LS-DYNA. The script reads the locations of each element, and determines for every element the convection and radiation boundary conditions based on trilinear interpolation of the results of the closest surrounding data points of the CFD.

With the convection and radiation as boundary conditions on every element, the thermal analysis can be run. The radiation and convection from the CFD are calculated up to 30 minutes, for the thermal analysis, longer simulation times are used to allow assessment of the behavior of the bridge for a longer fire duration

than 30 minutes. Therefore, after the 30 minutes, the convection and radiation boundary conditions are kept constant at the value they have at 30 minutes. This is a small limitation, but doesn't influence the result too much, since the HRR of the fire is already constant before this time. And the radiation and convection are also in a steady state at this time.

For the thermal analysis, no structural loads or constraints are applied on the model. The only goal of this analysis is to obtain the steel temperatures with respect to time.

8.1 Results for 2.1-meter distance

The resulting temperature distribution obtained from the thermal analysis after 30 minutes of fire for the 2.1-meter distance case can be seen in figure 8.2 and 8.1. The scale of the temperatures levels are the same for all 8 figures, ranging from 293.15 (20 °C) to 1000 K.

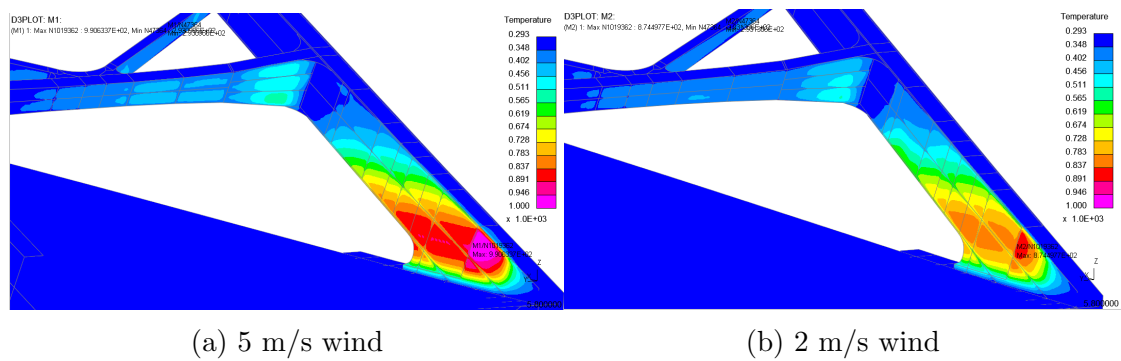


Figure 8.1: Predicted steel temperature, closed truck position 1, distance 2.1 m

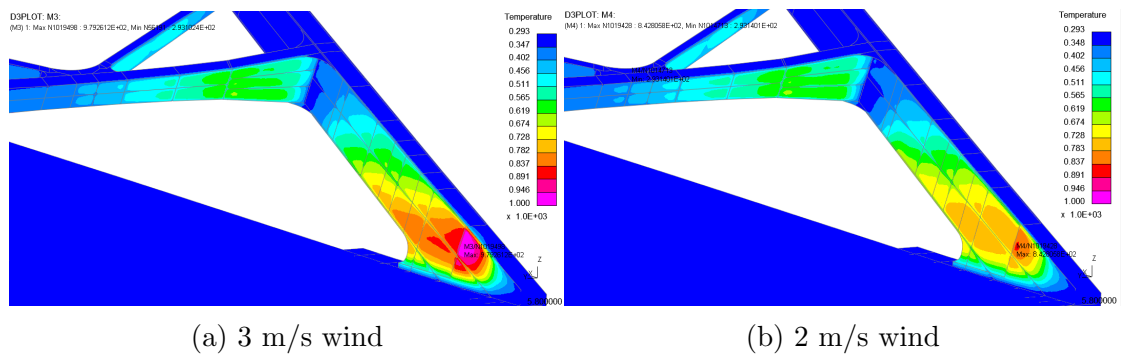
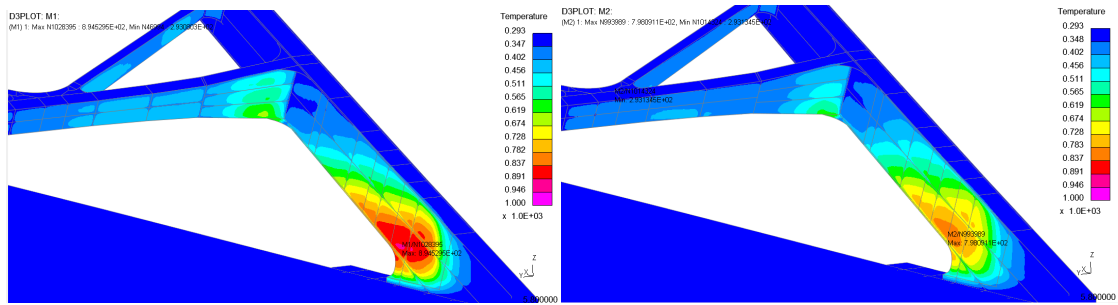


Figure 8.2: Predicted steel temperature, open truck position 1, distance 2.1 m

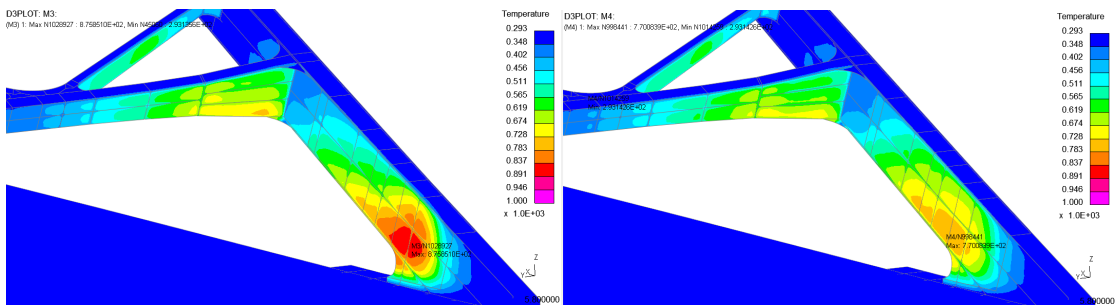
For position 2, the resulting temperatures can be seen in figure 8.4 and 8.3.



(a) 5 m/s wind

(b) 2 m/s wind

Figure 8.3: Predicted steel temperature, closed truck position 2, distance 2.1 m



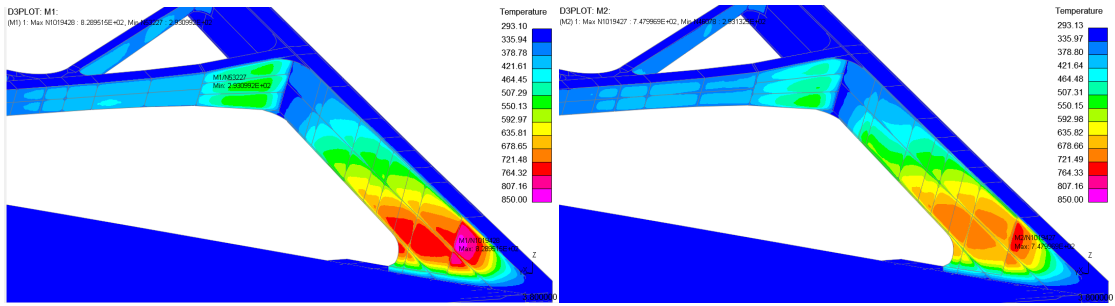
(a) 3 m/s wind

(b) 2 m/s wind

Figure 8.4: Predicted steel temperature, open truck position 2, distance 2.1 m

8.2 Results for 3.2 meter distance

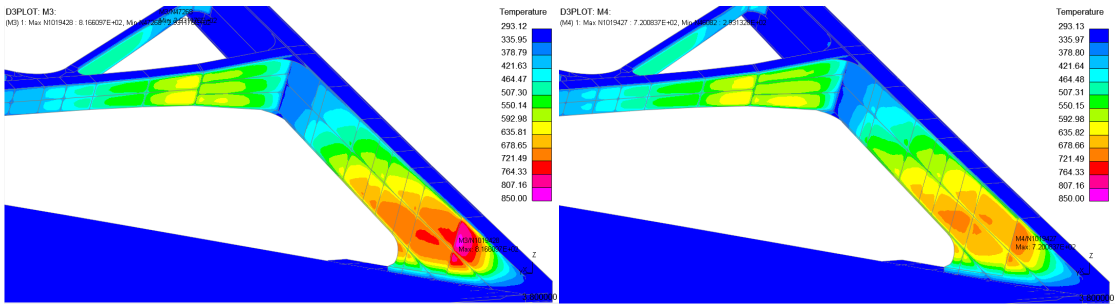
For the 3,2-meter distance case, the resulting temperature distribution after 30 minutes of fire can be seen in figure 8.6 and 8.5. The scale of the temperatures levels is the same for all figures of 3.2-meter distance, ranging from 293.15 to 850 K.



(a) 5 m/s wind

(b) 2 m/s wind

Figure 8.5: Predicted steel temperature, closed truck position 1, distance 3.2 m

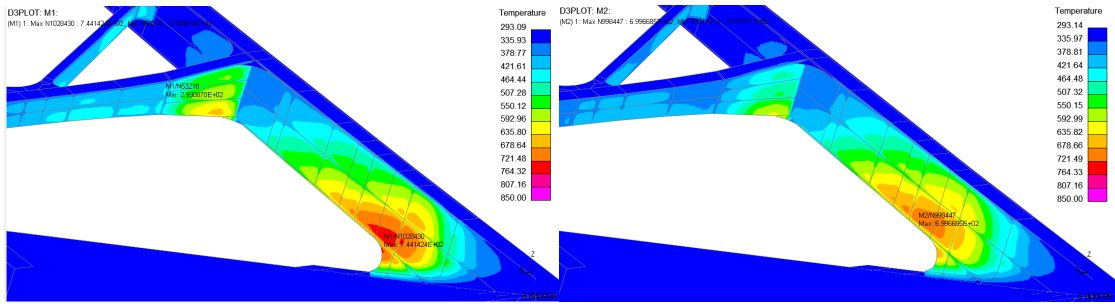


(a) 3 m/s wind

(b) 2 m/s wind

Figure 8.6: Predicted steel temperature, open truck position 1, distance 3.2 m

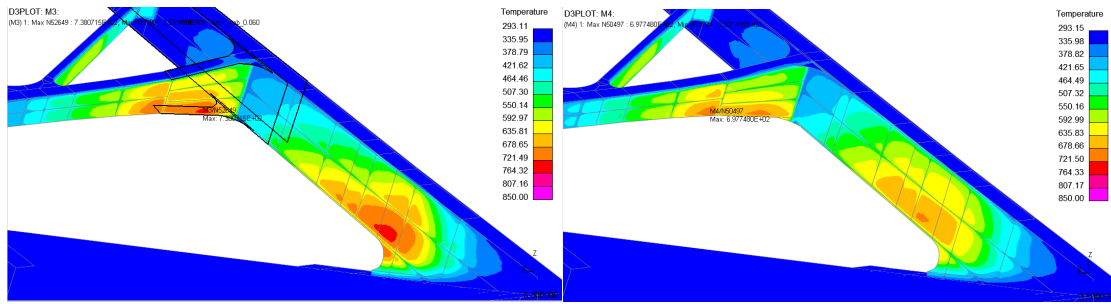
For position 2, the resulting temperatures can be seen in figure 8.8 and 8.7.



(a) 5 m/s wind

(b) 2 m/s wind

Figure 8.7: Predicted steel temperature, closed truck position 2, distance 3.2 m



(a) 3 m/s wind

(b) 2 m/s wind

Figure 8.8: Predicted steel temperature, open truck position 2, distance 3.2 m

8.3 Conclusions

The lateral distance has a quite significant effect on the temperatures. Figure 8.9 shows the maximum temperatures for the 8 different thermal analysis for both considered lateral distances. It also shows the difference in maximum temperatures between the 2 distances.

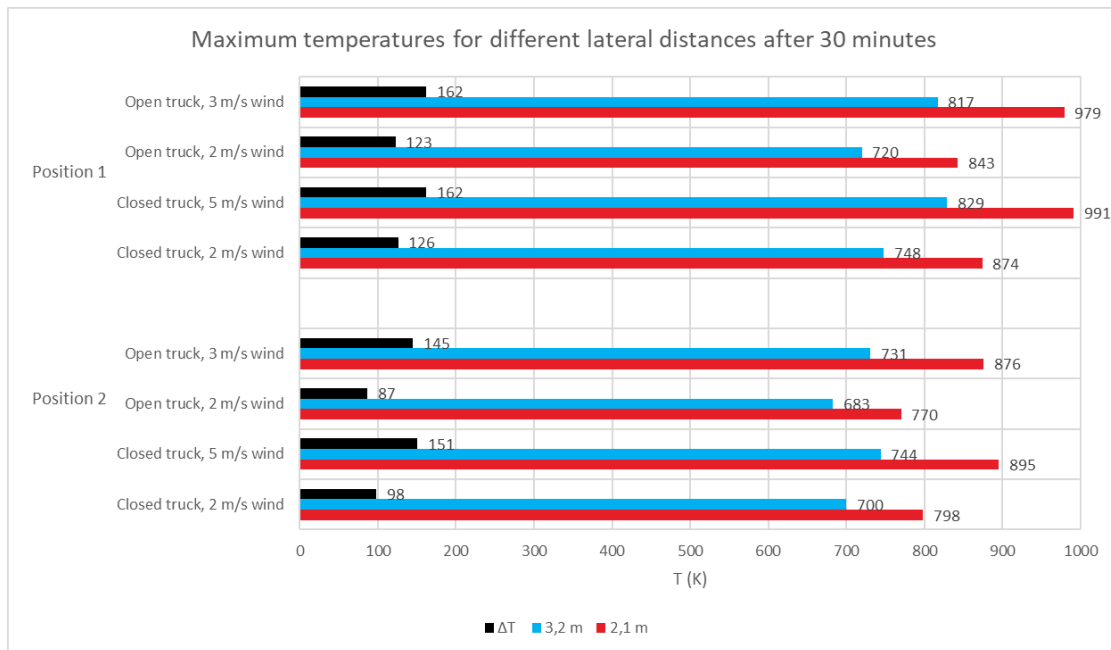


Figure 8.9: Maximum (arch) temperatures after 30 minutes for all fire scenarios

The images and graphs show that the wind fire interplay has a significant effect on the resulting steel temperatures, and some scenarios can be more critical than others. Higher wind speeds result in a higher peak temperature. However, lower

wind speeds result in higher temperatures in higher parts of the arch. When comparing open vs closed truck fires, it can be seen that open truck fires have a much bigger effect on the portal, while closed truck fires result in slightly higher peak temperatures for the arch.

By visual inspection of the temperature plots, and by comparing temperatures graphs at different location vs time, it can be concluded that some of the fire scenarios cannot be governing. The temperatures for the open truck 3 m/s wind are higher at every location for the first 30 minutes than for the closed truck 2 m/s wind scenario. So this fire scenario does not have to be investigated any further, since this cannot be critical.

The same holds for the 2 m/s open truck fire, some temperatures in these cases have slightly higher values in higher sections of the arch, but this is a very small region and at these locations, the temperatures are relatively low, which means not much strength and stiffness reduction is happening yet. In the rest of the arch and the portal, the open truck 3 m/s is governing over the open truck 2 m/s fire. And the maximum temperatures of the 3 m/s case are much higher than for the 2 m/s cases. The other 2 remaining fire scenarios still have a potential to be critical. These are the 5 m/s closed roof fire and the 3 m/s open roof fire. These are further considered in the full GMNIA analysis.

For both distances, and for each fire position and truck type, the difference in maximum temperature of the arch has been calculated as a result of different wind speeds. The results are shown in Table 4. The numbers in the table are the maximum temperature of the higher wind (hw) speed case minus the maximum temperature of the lower wind (lw) speed case.

Table 4: Difference in maximum temperature as a result of different wind speeds

	$T_{hw,max} - T_{lw,max}$	
	2.1 m	3.2 m
P1 Closed	116 °C	91 °C
P1 Open	137 °C	97 °C
P2 Closed	96 °C	44 °C
P2 Open	106 °C	48 °C

It can be seen from this table that the wind speed plays an important role in the resulting maximum temperatures of the steel, with higher winds resulting in increases of maximum temperature from 44 up to 137 degrees. Another conclusion that can be taken from this table , is that the influence of wind becomes more

significant when the distance of the truck to the arch reduces. As can be seen from the numbers under the 2.1 m column being significantly higher than under the 3.2 meter column. A final point that can be concluded here is that increasing the wind speed higher than 3 m/s does not have a significant effect on the temperatures anymore. For the open truck scenario's, a 3 m/s wind was compared to a 2 m/s wind, and for the closed truck scenario, this was a 5 m/s wind with a 2 m/s wind. However, the difference in temperature for the closed truck scenarios as a result of these different wind speeds is not higher (even lower) than for the open truck. Furthermore, the 5m/s closed truck scenario maximum temperatures are only slightly higher than the open 3 m/s scenario as can be seen in Table 5, while it was already concluded that a closed roof truck contributes to higher arch temperatures as well. This means increasing the wind speed beyond 3 m/s has very little extra effect.

Table 5: Maximum temperature difference between 5 m/s closed vs 3 m/s open

	$T_{max}(5 \text{ m/s}) - T_{max}(3 \text{ m/s})$	
	t=30 min	t=63 min
P1 2.1 m	11 °C	20 °C
P1 3.2 m	12 °C	7 °C
P2 2.1 m	19 °C	-4 °C
P2 3.2 m	60 °C	7 °C

Although the results of the thermal analysis give a good impression on the temperature distribution in the arch, the analysis have some limitations as well, these are described below:

- Radiation is only applied on bottom flange and inner web. In reality, the outer web and top flange could be influenced by heat as well, despite the effect being not nearly as big. This analysis assumes that the bridge geometry is blocking the flames from being visible to the top flange and outer web (View factor is 0).
- Convection is applied to all shells in the model. As previously mentioned, the bridge geometry is not modeled in the CFD analysis. This means temperatures at parts not facing the fire might be overestimated because of other bridge parts blocking the heat flow.
- Internal radiation between the webs is not taken into account, this assumption is checked in chapter 9.

9 Internal radiation check

While the inner web (web facing the fire) of the arch is heated directly by the fire, and is considered in detail in the GMNIA analysis, the outer web experiences a temperature increase as well. This happens by conduction of heat through the flanges and due to internal radiation between surfaces within a structural section. The conduction part is included in the model, since the thermal conductivity is specified in the model and allows for heat flow through the material. The radiation part is not included in the GMNIA model. The effect of this is checked here with a separate calculation.

Heating of an object, in this case steel, is given by the following equation

$$\rho_a V c_a(T) \frac{dT}{dt} = \sum q \quad (14)$$

$\sum q$ = Sum of the heat fluxes [W]

When taking only the radiative heat into account, this sum of the heat fluxes becomes:

$$\rho_a V c_a(T) \frac{dT}{dt} = A \phi \varepsilon \sigma (T_1^4(t) - T^4) \quad (15)$$

Both sides can be divided by the Area which results in:

$$\rho_a t_p c_a(T) \frac{dT}{dt} = \Phi \varepsilon \sigma (T_1^4(t) - T^4) \quad (16)$$

t_p = plate thickness [m]

$\varepsilon = 1$

T_1 = Temperature of the inner flange [K]

T = Unknown temperature of the outer web [K]

This is a nonlinear ordinary differential equation (ODE) that can be solved by approximating the temperature gradient by forward finite differences.

$$\rho_a t_p c_a(T) \frac{\Delta T}{\Delta t} = \Phi \varepsilon \sigma (T_1^4(t) - T^4) \quad (17)$$

$$\Delta T = \frac{\Phi \varepsilon \sigma (T_1^4(t) - T^4)}{\rho_a t_p c_a(T)} \cdot \Delta t \quad (18)$$

$$\Delta T = T(t_{i+1}) - T(t_i) \quad (19)$$

$$T(t_{i+1}) = T(t_i) + \frac{\Phi \varepsilon \sigma (T_1^4(t_i) - T^4(t_i))}{\rho_a t_p c_a(T(t_i))} \cdot \Delta t \quad (20)$$

The temperature of the inner flange at each time step is known from the CFD analysis. With equation 20, the new temperature at every time step can be calculated based on the known temperatures of the previous time step. At $t=0$, the temperature is set to 293.15 K (20°C).

For the calculation of the view factor, a standard case of 2 parallel strips which represent the 2 webs of the arch section has been used, as shown in figure 9.1.

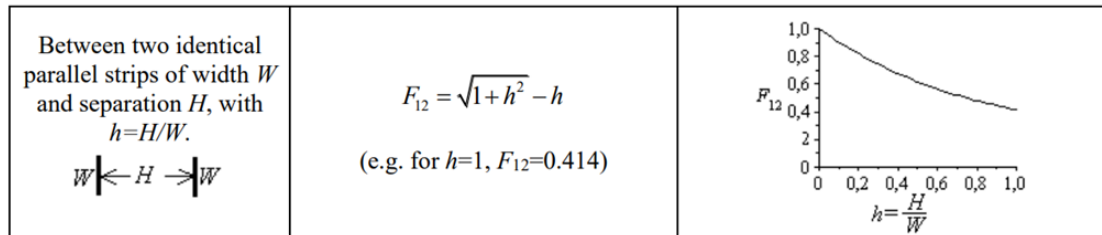


Figure 9.1: View factor for 2 parallel strips (From [15])

$$h = \frac{H}{W} = \frac{1.2}{3.5} = 0.34$$

$$\Phi = F = \sqrt{1+h^2} - h = 0.714$$

The temperature of the inner web has been assumed to be the same for the whole web at every time step, even though in reality, and from the results of the CFD, it is not. For this inner web temperature, a temperature curve has been extracted for the node with the highest temperature in the LS-DYNA model.

Equation 20 can now be used to calculate the outer web (web not facing the fire) Temperature. The result is shown in figure 9.2

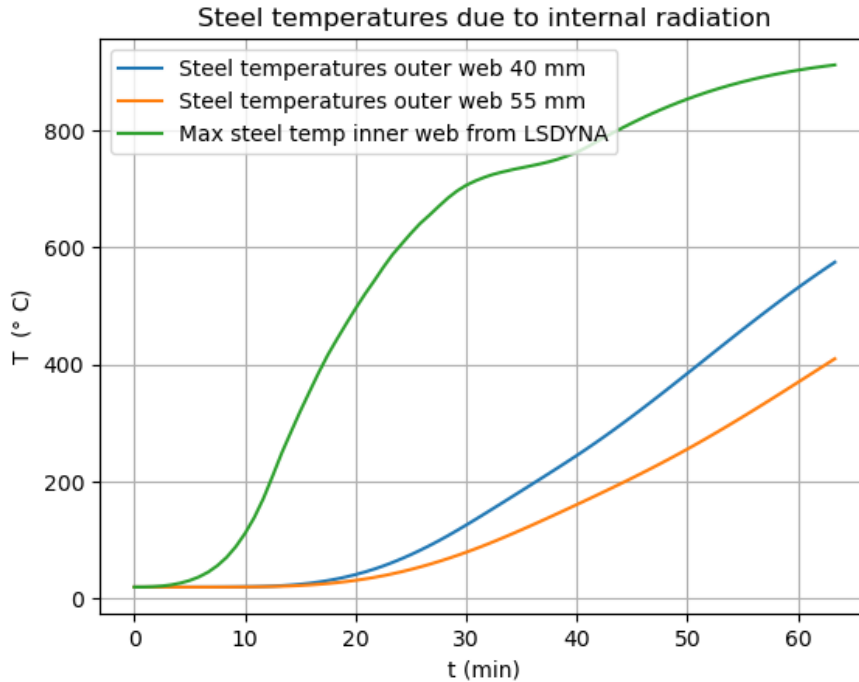


Figure 9.2: Temperature of the outer web due to internal radiation

After 30 minutes, the maximum temperature in the outer web (web not facing the fire) due to internal radiation is 117 °C for the sections with a thickness of 40 mm and 74 °C for the sections of 55 mm. For steel CSC 4 sections, the Young's modulus and yield stress start to reduce from 100 °C. This increased temperature is very close to this limit, so barely any strength reduction is happening yet. The internal radiation will thus not be taken into account in further analysis. When a longer duration than 30 minutes is considered. The effect becomes significant, and this internal radiation does need to be taken into account.

Assumptions made in this analysis:

- Whole inner web assumed to be the same temperature as the node with the maximum temperature. In reality, the temperatures of other parts/nodes of the inner web would be lower and with that, the radiation as well. So, this is conservative.
- Temperature curve extracted from one fire scenario (open truck 3m/s wind), other fire scenarios might give a higher maximum temperature for the inner web. This is a limitation, but the purpose of this analysis is to show that the internal surface radiation is not significant and does not have to be considered in further analysis. This is still the case for different fire scenarios.

- Conduction through the thickness of the webs is not accounted for. It is assumed that both sides of the web have the same temperature over time. In reality, this conduction through the thickness takes a bit of time, which means the radiative heat from the inner web is lower (temperature of the inside of the web has a delay on the temperature on the outside). This is also a conservative assumption.
- Effects of radiation is considered separately, temperature increase due to conduction through the flanges happens simultaneously. This conduction is included in the GMNIA analysis.
- Inner web temperatures are based on CFD results, when EC curves are used to determine steel temperatures, the internal radiation and temperatures in the outer web will be much higher as well.

10 Buckling analysis

For the buckling analysis, the material properties are used, without thermal strength reduction. An investigation has been done to validate if this makes a significant difference, but this is not the case, this is as discussed in Appendix C with the test model. The buckling analysis is performed for the two different accidental load combinations. It is expected that the buckling mode will have little influence on the failure mechanism and load, since the thermal expansion and strength properties reduction govern this in the design. A small investigation is done to see the effect of different buckling modes used as imperfections.

These load combinations are determined with Eurocode 1990 [18] and the ψ factors are from the Dutch national annex [19]. The resulting load combinations are:

$$G_{k,j} + A_d + 0.8 \cdot Q_{traffic} \quad (21)$$

$$G_{k,j} + A_d + 0.6 \cdot Q_{wind} + 0.4 \cdot Q_{traffic} \quad (22)$$

These two load combination will be referred to as traffic leading (Eq. 21) and wind leading (Eq. 22)

10.1 Traffic leading

For the buckling analysis with the traffic leading Load Combination (LC), 100 eigenvalues are computed. The buckling mode that is used for the imperfection is the first buckling mode that is located in the area that is affected by the fire. The first buckling mode that was in the affected are has a load factor of 4.24, the buckling mode can be seen in figure 10.1.

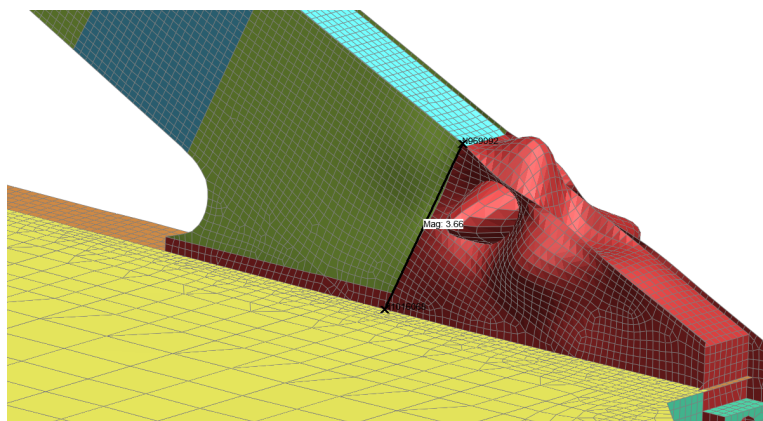


Figure 10.1: Buckling mode for the traffic leading LC

The maximum size of the imperfection is scaled to the length of the shortest span of the plate, which is measured in the model and can be seen in figure 10.1, this is 3.66 meter. The size of the imperfection is calculated according to NEN-EN 1993-1-5 and for local plate buckling this is $\min(a/200, b/200)$ where a and b are the plate dimensions as shown in figure 10.2. So in this case the imperfection size is $3.66/200 = 0.0183$ m or 18.3 mm.

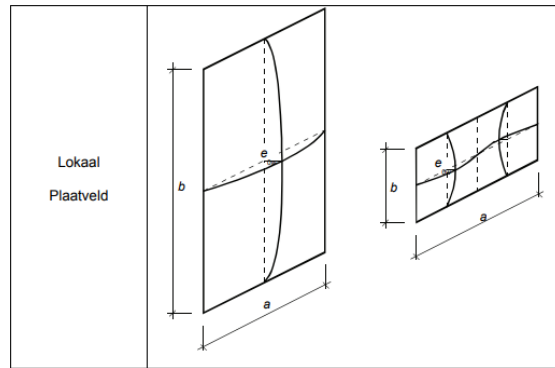


Figure 10.2: Dimensions for calculating imperfection size

10.2 Wind leading

For the buckling analysis with wind leading LC, it was necessary to compute the first 200 eigenvalues, since the first 100 did not show a buckling mode in the area that is affected by the fire. The first buckling mode that was in the affected area has a load factor of 4.49, this mode can be seen in figure 10.3

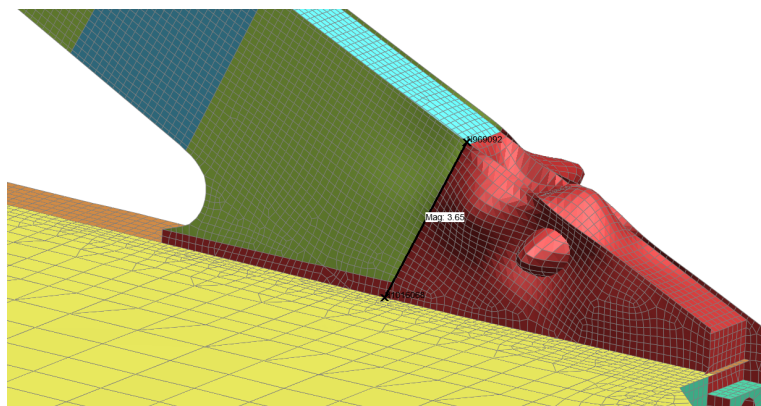


Figure 10.3: Buckling mode for the wind leading LC

The maximum size of the imperfection is the same as for the traffic leading case.

Both of the buckling analysis show a lot of local buckling modes. but no global buckling modes are obtained, this means the buckling factors for the global buckling modes are relatively high, in this case, at least higher than 9.0 for the traffic leading and 7.5 for the wind leading. These global buckling modes are therefore not considered.

10.3 Effect of imperfections

A small study has been performed to investigate the effect of imperfections. For this, 3 different GMNIA analysis have been done for the same model with different imperfections. One of the models did not have any imperfections modelled. The other imperfections can be seen in figure 10.1 (imperfection 1) and 10.4 (imperfection 2).

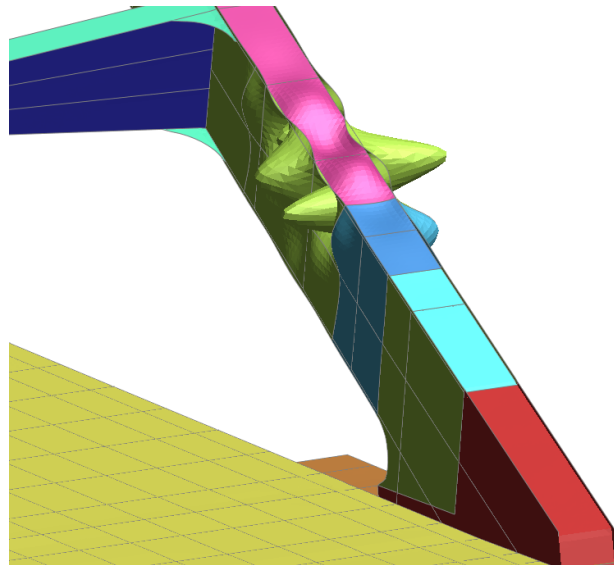


Figure 10.4: Different (higher) buckling mode at fire location for traffic leading LC

From the resulting stresses and strains, it can be concluded that the influence of imperfections is very small, these results are given in Appendix F. Modeling imperfections in general has very little effect on the outcome, and so does the location of the imperfections. This means the imperfections do not much interact with the heating, deformations and buckling behavior is governed by the thermal expansion and reduced material properties. Therefore, not much attention will be given to these buckling modes. Imperfections will be included, but not all models are checked for different imperfections and modes.

11 GMNIA analysis

With the results of the thermal and buckling analysis, different sets of full GMNIA analysis can be performed. The analysis can be done for every thermal and load combination. However, not every possible combination will be run. Separate investigations are done to investigate the effect of different parameters. These include: The longitudinal position of the fire, the lateral position of the fire, the difference due to different fire scenarios and the difference for the two load combinations. These investigations will then result in the most critical fire scenario for this bridge. Next to the performance based models, a full GMNIA analysis will be done with the previously determined steel temperatures based on Eurocode.

In the GMNIA models, failure is defined as the moment at which the plastic strain limit is reached. After the plastic strain limit is reached, the elements are removed from the finite element model. The plastic strain limit is set to 5% in the models, this is a limit that may be used for non-linear FEM models according to prEN 1993-1-14 [26]. The removal of elements in the model after reaching the plastic strain limit is referred to as plastic failure.

11.1 Bridge capacity with prescriptive thermal load applied

Aside from determining the structure's capacity with realistic fire scenario, the capacity of the structure has been determined using the steel temperatures over time as determined with Eurocode. The FEM model has still been used to determine the structure its capacity, since the structure is too complicated to do this with hand calculations.

For the different steel section thicknesses, the different temperatures have been applied as thermal boundary conditions. They have been applied on the same sections for which the radiation boundary conditions were applied in the thermal models, so on the bottom flanges and the inner webs of the arch. Two different cases are still distinguished here. One where the portal is also thermally loaded up to half the width of the bridge, and one where this is not the case and only the arch is loaded.

The locations where steel temperatures are applied as thermal boundary conditions are shown in figure 11.1. These are temperatures after 30 minutes of the Hydrocarbon fire. The figure also clearly shows how different section thicknesses have different temperatures after a certain amount of time.

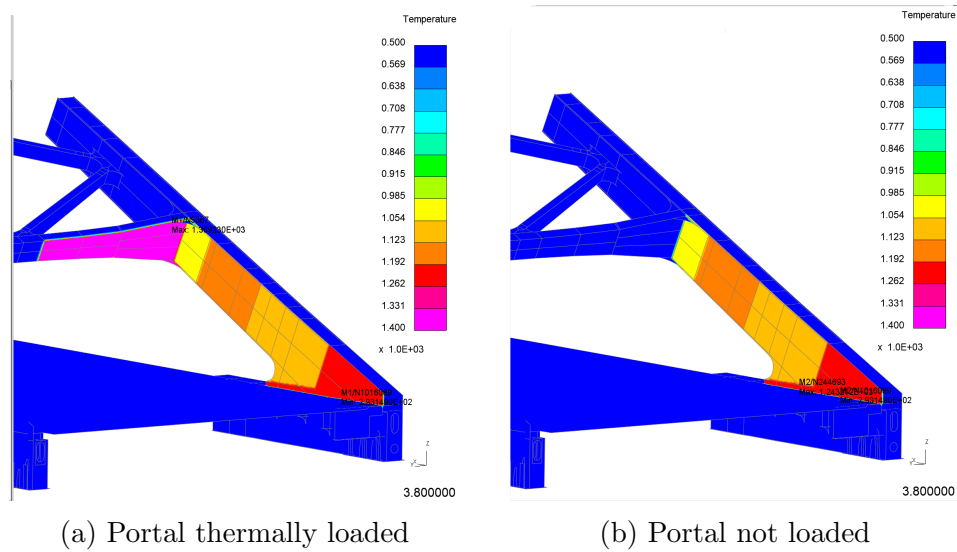


Figure 11.1: Temperatures (K) calculated from Eurocode

The portal has relatively thin sections, this is why the temperatures in the portal rise very quickly and are very high at early moment in time. However, in these temperature calculations, the view factor has been assumed to be 1.0. For some parts of the arch this is a reasonable assumption (although still conservative), but for the portal, which is at quite a bit of distance from the fire. This might be too conservative. This is why one scenario without loading the portal has been considered as well. A more correct scenario would be somewhere between these two.

When looking at the GMNIA analysis of these scenarios, it can be seen that in both cases, the bridge fails before the required 30 minute resistance. The result for the 2 different scenarios are quite similar. For the portal included scenario, the plastic failure strain is reached after 15 minutes, whereas the other scenario this is reached after 16 min. The location of the plastic failure strain is the same. The stresses and strains in the arch section after 30 minutes are quite similar, although some deviations can be seen in the stresses in the upper flange of the arch. These are shown in figure 11.2 and 11.3

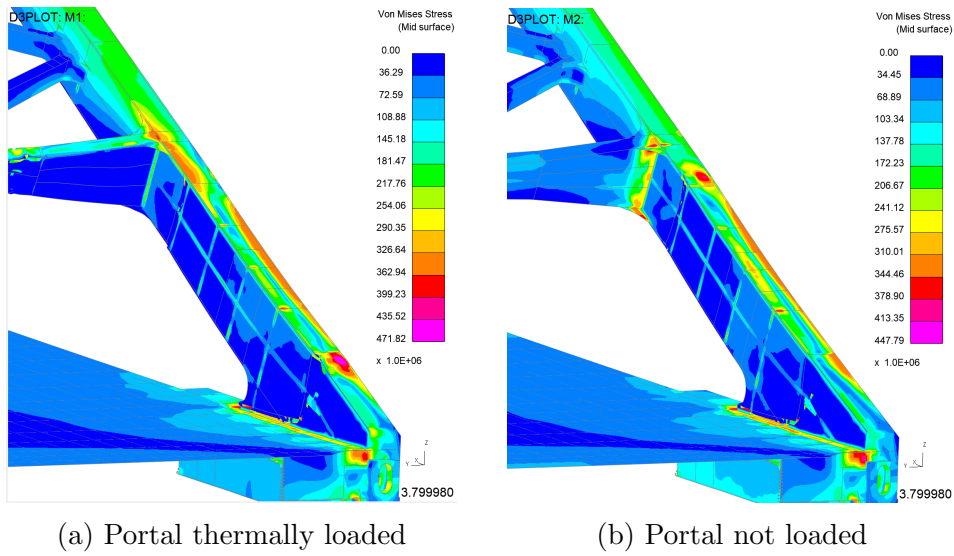


Figure 11.2: Von Mises Stresses (N/m^2)

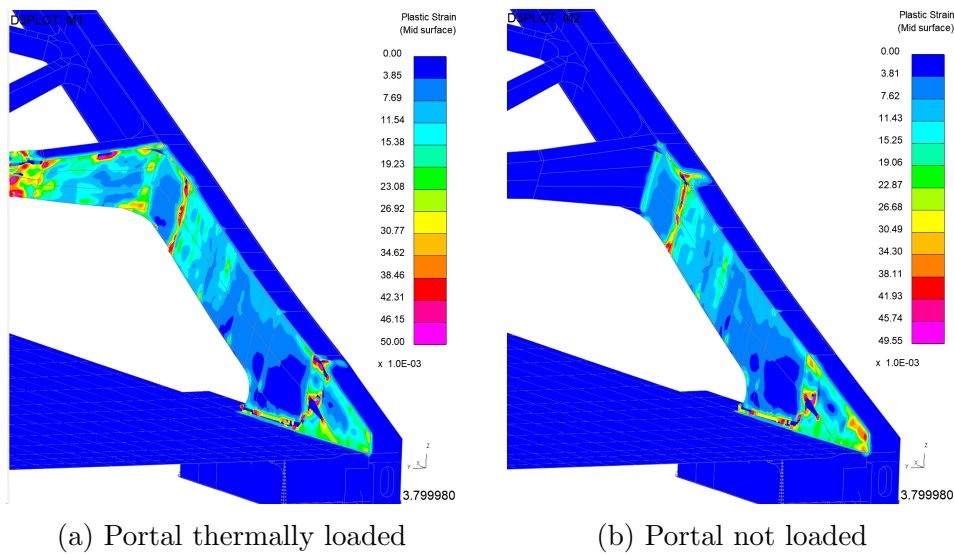


Figure 11.3: Plastic strain (-)

The stresses and strains in the portal are different here. In the case where the portal is thermally loaded, all the strength in the portal flange is already lost, so no stresses can be taken there, which explains why the Von Mises (VM) stresses are 0 there. The plastic strains in the case are much higher for the case where the portal is loaded, this is because the thermal expansion in combination with the reduced strength caused the portal to buckle at a very early stage (approximately

5 minutes).

When looking beyond the 30 minutes, the plastic strain failure develops and eventually leads to complete collapse of the bridge. Some differences in behavior occur here. The buckling locations start to differ a bit, eventually leading to different positions where full collapse initiates. These buckled shape before failure and the locations where the buckling behavior differs are shown in figure 11.4. The deformations in this image are magnified by a factor 5 to improve visibility.

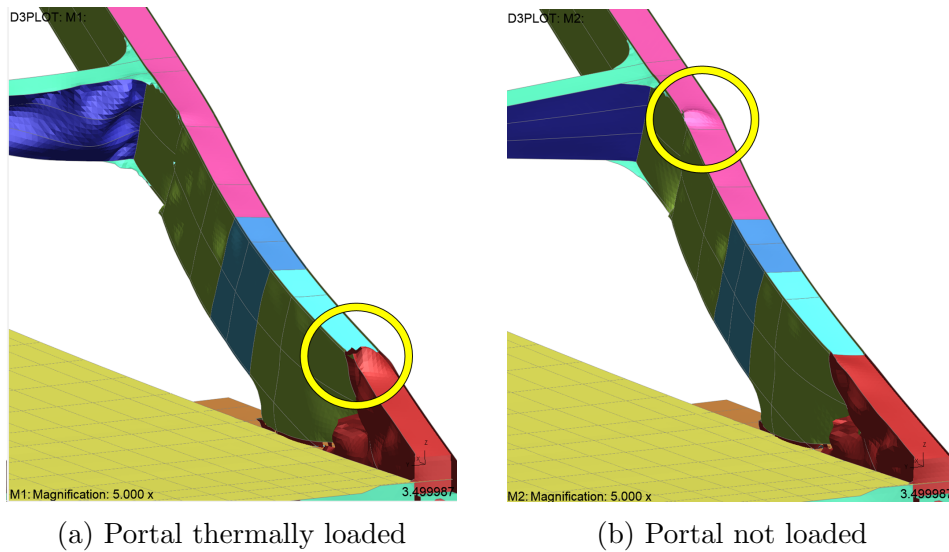


Figure 11.4: Buckling behavior (Deformation 5x magnified)

After the collapse is initiated by buckling of the highlighted locations, other locations start to buckle and fail as well, progressively leading to full collapse. Figure 11.5 shows the bridge at the end of the analysis when fully failed (no magnification).

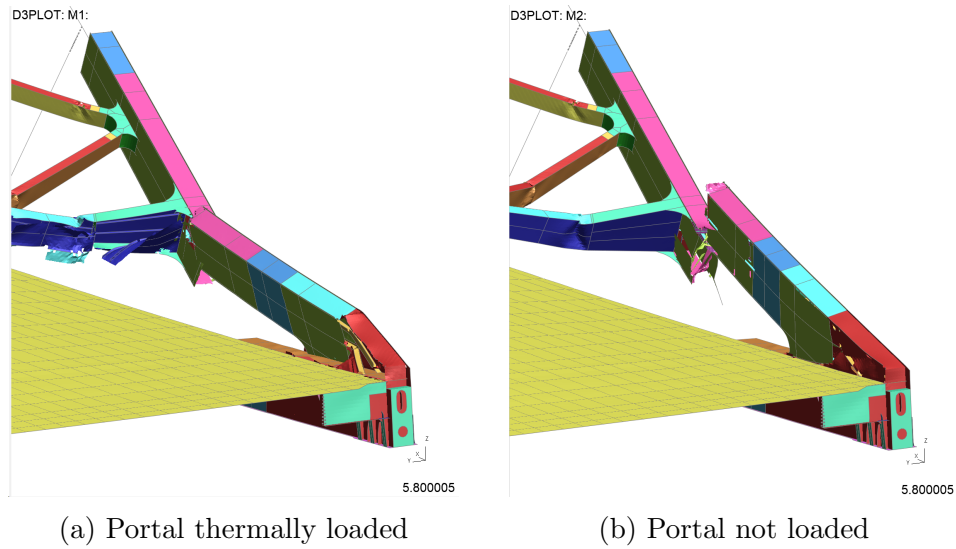


Figure 11.5: Bridge fully failed

Two things can be concluded from these partly code based analyses. First, applying fires scenarios from Eurocode leads to failure of the bridge (without fire protection). And second, heating of the portal in addition to the arch has big influence on the resulting failure mode, but the failure times are still similar, as the time for first plastic failure is 15 minutes vs 16 minutes with and without the portal loading respectively.

Protection is thus necessary when applying prescriptive temperatures. To determine this amount of protection, an iterative process is performed where the section temperature of the failing sections are extracted from the model at the time of failure, the amount of protection is then calculated such that this temperature is reached after 30 minutes. The model is then rerun with the new temperature boundaries that are obtained after applying protection. For this model, 4 iterations were needed to increase the failure time from 15 to 31 min. The amount of protection required for each of the sections is shown in table 6. Both the wind and traffic load combination have been checked and both sustain the 30-minute fire given these protection thicknesses.

Table 6: Required protection thicknesses

Section thickness (mm)	Protective layer thickness (mm)
40	1.0
50	0.8
55	0.6
60	0.4
70	0

When looking at the temperature plot over time for the different sections after all iterations have been done, which can be seen in figure 11.6, it is interesting to see that the temperature gradients are very similar for all parts of the web even for different thicknesses. This suggests that, for this case study, the critical temperature is around 873 K (600 °C) (Note that this will be different when the outer web and top flange are thermally loaded as well, but in this case study it is assumed that these are not affected by the fire).

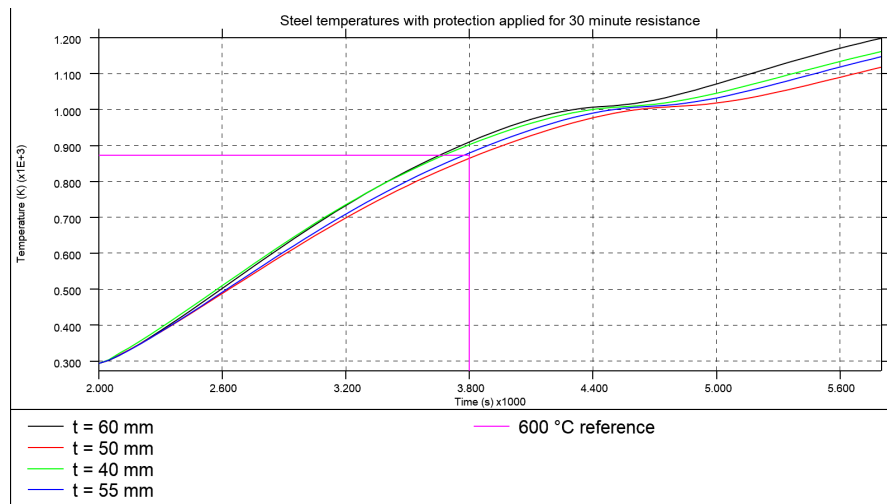


Figure 11.6: Temperature vs time of different steel sections with protection

The total intumescent protection volume for each ASP with this calculation method = $0.0587 \text{ m}^3 = 58.7 \text{ L}$. This is 4.1 times less than what was calculated based on the 350 °C limit. Taking this 350 °C is thus very conservative and is not recommended for economical design.

The protection method used for calculations is intumescent paint, there are however other methods to improve fire resistivity, one of these methods is increasing the steel thickness. This method is shortly discussed in Appendix G, where this

measure is both tested for the Eurocode applied temperatures and for the most critical performance based scenario.

11.2 Different fire scenario

Now, results from the detailed performance based analysis will be discussed, where temperatures are based on the results from the CFD analysis.

When comparing fire position 1 with fire position 2, a clear difference in behavior can be seen. The buckling develops at a different location due to the different thermal profiles. Resulting in quite a different failure mode. This can be seen in the difference between figure 11.7a and 11.8a and between 11.7b and 11.8b.

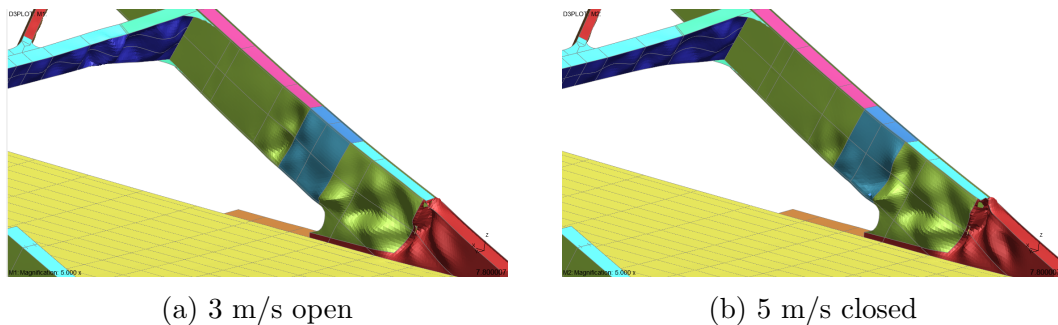


Figure 11.7: Buckling behavior for fire position 1 (5x magnified deformation)

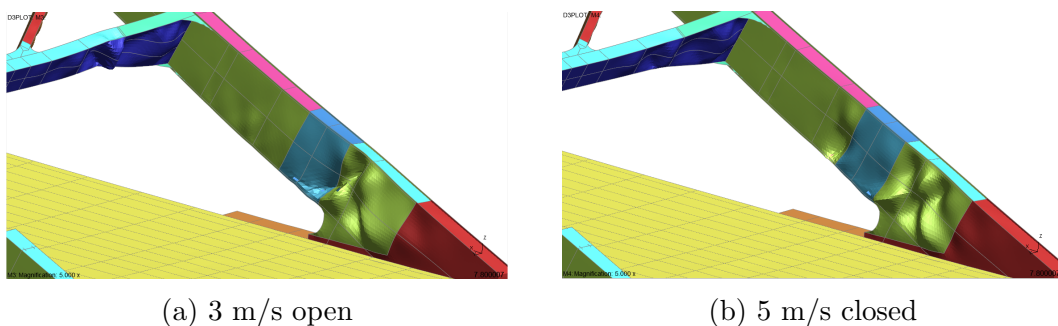


Figure 11.8: Buckling behavior for fire position 2 (5x magnified deformation)

Some small differences in buckling behavior can also be seen when comparing the 3m/s open scenario with the 5 m/s closed scenario, but overall, these scenarios behave quite similar. The main differences here are caused by the influence of the portal that is much more affected in the 3 m/s open scenario, as was also the reason for the differences for the 2 Eurocode fire analysis.

For these 4 different scenarios, the time to reach plastic failure has been obtained. The results are given in table 7. These are all for the traffic leading scenario

Table 7: Time to reach plastic failure strain traffic leading

	Position 1	Position 2
Open 3 m/s wind	35 min	43 min *
Closed 5 m/s wind	39 min	47 min

*Plastic failure strain in portal is reached after 32 min but here only the times for the arch are considered

From these times it can be seen that position 1 is more critical than position 2, reaching plastic failure 8 minutes faster in both scenarios. These times to reach plastic failure show that the open truck fire scenario is more critical than the closed truck fire, since this failure strain is reached 4 minutes earlier for both positions. The peak temperatures are higher for the closed truck scenario, so the only reason that the open truck scenario is more critical, is that the strength of the portal plays a significant effect in the resulting failure time as well.

11.3 Different lateral fire locations

Of course, when the distance from the fire to the arch is reduced, the result is an increase in temperature. This section will however compare stresses, strains, and buckling states for the different distances at different times.

For both considered longitudinal fire positions, changing the lateral position does not change the buckling mode.

In none of these scenarios where the lateral distance is 3.2 meter did the bridge start failing. This means that moving the fire laterally by only 1.1 meter already has a huge impact on the resulting capacity. This is because the intensity of the radiation decreases with the square of the distances according to the inverse square law: given in equation 23.

$$I = k/d^2 \tag{23}$$

Where:

I is the intensity of radiation

k is a constant (depending on the intensity)

d is the distance

Reducing the distance from 3.2 to 2.1 meter, which a reduction of a factor 1.5, will thus result in a radiation increase of a factor 2.3. This inverse squared distance relation makes the lateral distance one of the most important variables in fire resistance design.

Furthermore, the Von Mises stresses after 30 minutes have been obtained for the different fire scenarios with the lateral distance of 2.1 m. For each of these fire scenarios, a similar stress state has then been found for the 3.2 meter lateral distance cases, which occurs at a different (later) time. This gives an indication of the minimum extra time the bridge is able to withstand the fire.

Figure 11.9 shows similar stress states for the open truck 3 m/s wind fire scenario for position 1. The time for the 3.2 meter scenario here is 46 minutes after the start of the fire, this similar stress state as for the 2.1-meter distance case is thus reached 16 minutes later. For the other fire scenarios, these similar stress states are reached at the same times.

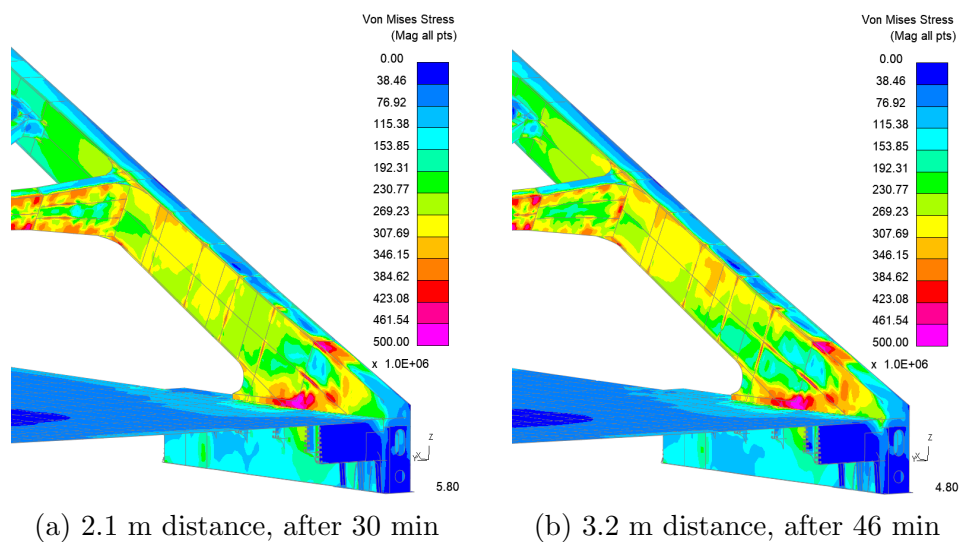


Figure 11.9: Open truck position 1 stress states comparison

Similar stress states for the other fire scenarios were found with a 16 minutes time difference. This 16 minutes is not the extra time the bridge can survive (this is even longer), but just an indication of how much longer it takes to get to the same state when the lateral distance is increased. The maximum temperature that can be reached is much lower when the distance is increased.

11.4 Different longitudinal fire locations

Aside from fire position 1 and 2, which are investigated in detail, different longitudinal fire positions have been explored around the arch. It was investigated whether moving the truck more towards the portal, or more towards the back of the bridge would make a significant difference.

When the middle of the fire is moved more towards the portal, the radiation under the portal increases compared to just the end of the truck being under the portal. Therefore, a longitudinal shift of 2 m and 6 m (position 3 and 4) as shown in figure 11.10 towards the portal have been applied and investigated. The thermal analysis showed that there was indeed an increase in maximum temperatures of the portal.

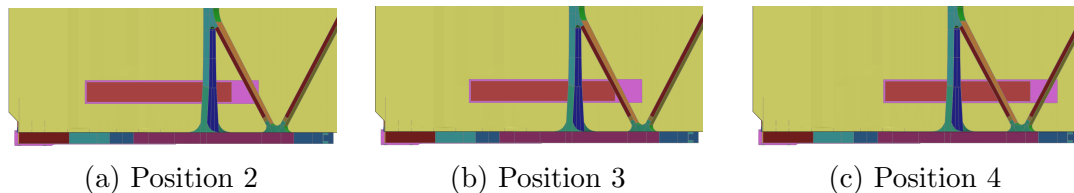


Figure 11.10: Top view of different positions of truck shifted towards portal (lateral distance 3.2 m)

When looking at the GMNIA results however, it can be seen this shift has very little influence on the stresses and strains in the portal. This is shown in figures 11.11 up to 11.12b. These are the result after 63 minutes. It can be seen that the plastic strains in the portal are almost the same. This is because this section of the portal is relatively thin (14 mm), and therefore, its strength contribution is already very low under the thermal conditions in position 2. Moving the truck further under the portal only reduced the temperatures and the strains in the arch, as can also be seen from the figures. Therefore, these scenarios are not critical and do not need to be considered further.

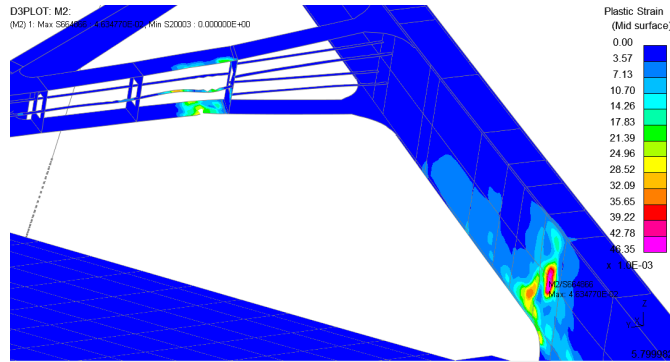
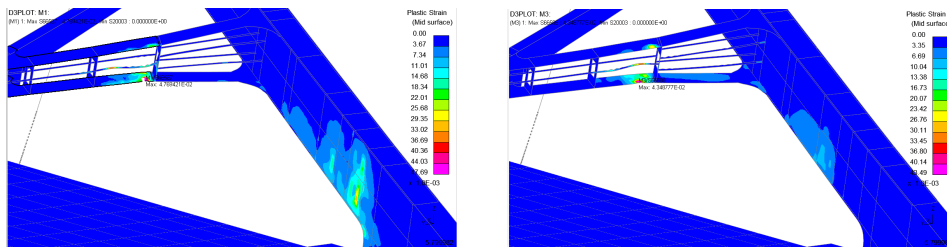


Figure 11.11: Plastic strain (-) position 2 after 63 minutes of fire

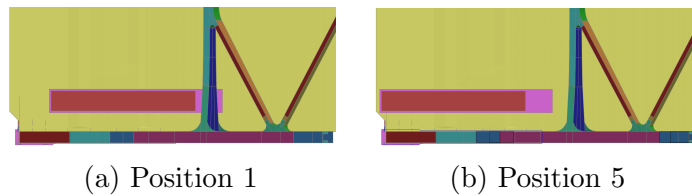


(a) Position 3

(b) Position 4

Figure 11.12: Plastic strain (-) after 63 minutes of fire

A similar comparison has been done by moving the truck 4 meter towards the back of the bridge from position 1 (position 5) as shown in figure 11.13.



(a) Position 1

(b) Position 5

Figure 11.13: Top view of different positions of truck shifted towards the back (lateral distance 2.1 m)

Figure 11.14 shows the plastic strains for position 1 and position 5 after 30 minutes of fire (This comparison has been done with the 2.1 m lateral distance).

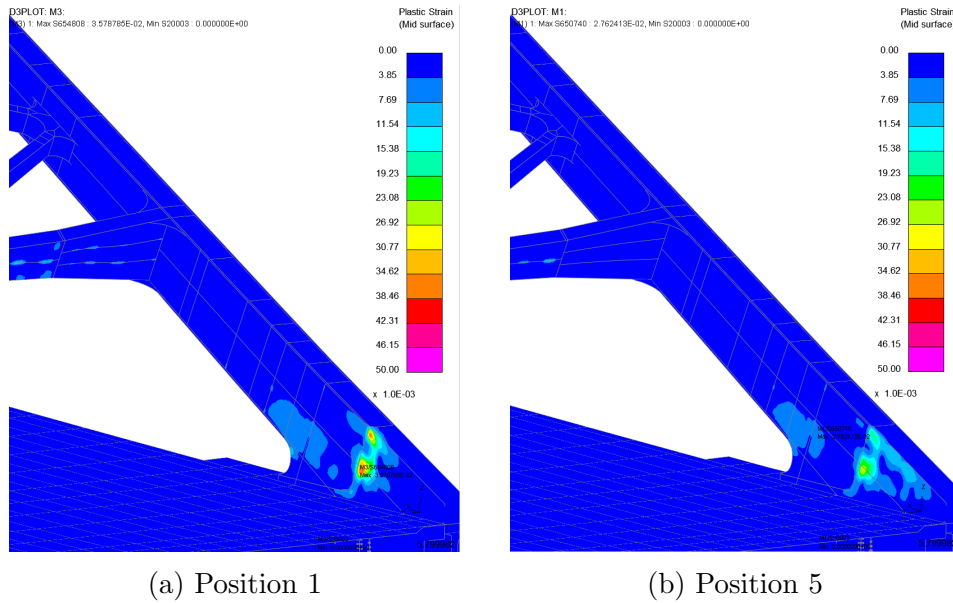


Figure 11.14: Plastic strain (-) after 30 minutes of fire

At the end of the analysis (63 minutes), the bridge in the position 5 scenario is at the plastic failure strain, but has not failed yet. With position 1, plastic failure is reached after 35 minutes. This difference in strain after 30 minutes together with the difference in failure times shows that moving the truck backwards will not result in a more critical scenario. so that position will not be considered any further either.

11.5 Live load influence

To investigate the difference due to different live loads, the same 4 fire scenarios have been considered as in section 11.2, but now with the wind leading load combination. The times to reach plastic failure has been obtained again, these are shown in table 8.

Table 8: Time to reach plastic failure strain wind leading

	Position 1	Position 2
Open 3 m/s wind	30 min	44 min*
Closed 5 m/s wind	31 min	52 min

*Plastic failure strain in portal is reached after 26.7 min but here only the times for the arch are considered

Figure 11.15 shows the buckling behavior for both the wind leading and traffic

leading load combination. The location is the same, but there are some differences in the shape, especially in the lower parts of the arch.

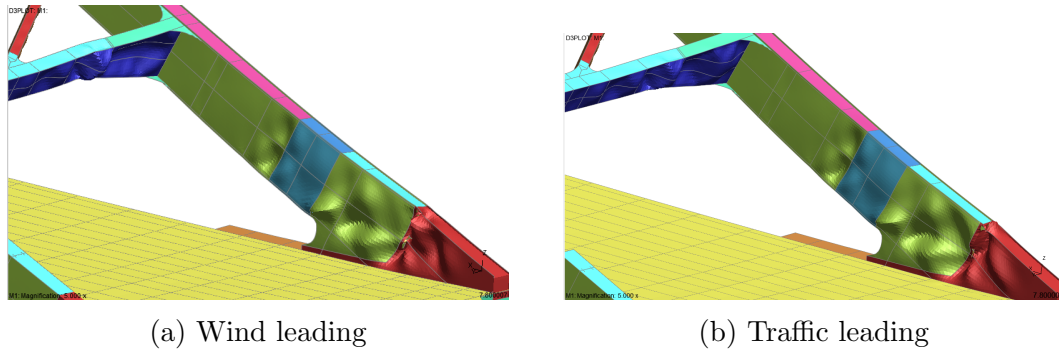


Figure 11.15: Buckling behavior for fire position 1 3m/s open

The conclusion from this comparison is that live loads that are applied are very important. Both the failure time and the buckling behavior differ for the 2 applied load combinations. Different load combinations are critical for different positions. For this case study, wind leading is governing for position 1 and traffic leading for position 2.

So, even though without fire present, a certain single load combination can be critical, it can be that another load combination results in higher stresses around the location of the fire, which makes that combination more critical in a fire scenario. This means it is always important to consider all possible critical load combinations.

11.6 Conclusions

When all comparisons taken in the detailed performance based GMNIA analysis are taken into account, there are only a couple of scenarios that can be critical. For this case study, the most critical scenario is the open truck 3 m/s wind fire scenario where the truck is at a distance of 2.1 meters from the arch, for either the wind leading load combination. For all the performance based analysis performed, the failure time was at least 30 minutes, meaning no protection is necessary for the critical design fire in this case study. When Eurocode temperature loads are applied, protection is necessary.

12 Comparison of methods

12.1 Prescriptive and performance based comparison

This research shows that doing a detailed thermal structural analysis of fire on a steel bridge can indeed lead to material savings. The performance based analyses show that the bridge does not fail in every fire scenario for at least 30 minutes, and even survives (no collapse) for longer after some elements in the model have failed. When applying temperatures based on Eurocode, failure is reached after 15 minutes. The Eurocode method thus results in the conclusion that fire protection is necessary on the bridge, while the performance based analysis shows that it is not.

The main reason for these differences in results are related to the input of the performance based and the prescriptive analysis. First, the fire scenario is different. The performance based method uses a heavy good vehicle with an ultra-fast growth rate as the design fire scenario, which is based on a probabilistic analysis. The prescriptive method from the Eurocode uses temperatures as input that are based on the hydrocarbon fire curve. These are 2 very different scenarios, which is one of the reasons for the differences in result.

The second main difference is that the location of the Eurocode fire is not specified, it is assumed that the fire is present everywhere and that all view factors are 1, implying the fire is everywhere. In the performance based case, the fire is modeled in a specific location, resulting in just a localized part of the bridge that is highly affected, and parts that are further away from the fire being less affected.

A way to bridge the difference in results between these two methods is by creating a new artificial 'Eurocode' temperature curve. The current Eurocode guidelines do not have different fire curves for different fire scenarios in (steel) bridge design. Creating one that matches the design fire scenario can lead to a much less conservative design. In this approach, the temperature curve is adjusted such that the resulting steel temperatures are matching the maximum steel temperatures of the detailed analysis. These adjusted curves change for different lateral distances (and fire scenarios), since a different lateral distance in the detailed analysis also results in different maxima. With this method, the adjusted temperature curves have been created and tuned to match the results of the detailed analysis for 2.1 and 3.2 m lateral distance (For the open truck 3 m/s wind case, which is shown to be the most critical). The shape of the curves match the shape of the heat release rate curve that was used in FDS, with a t-squared increase in temperature with constant temperature after its maximum is reached. The adjusted temperature as

a function of time plotted together with the hydrocarbon fire curve can be seen in figure 12.1

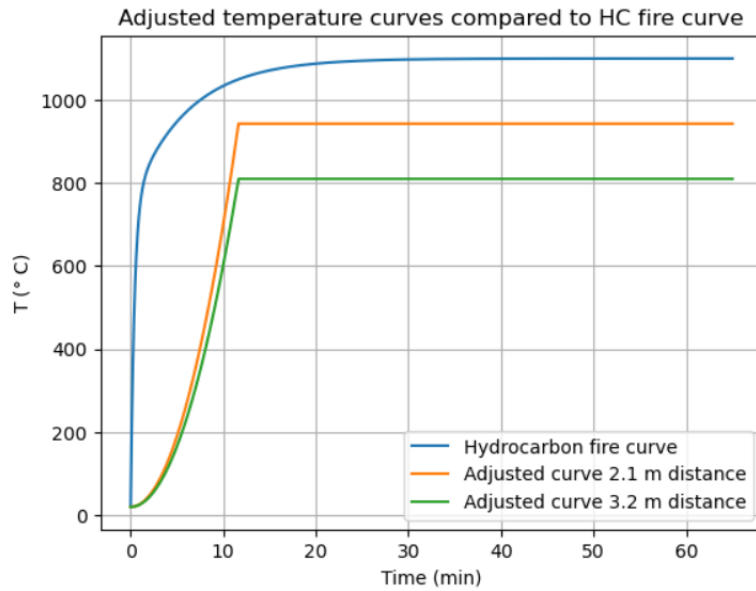


Figure 12.1: New adjusted temperature curves

To obtain the LS-DYNA temperatures from the detailed analyses, which are used for validating these adjusted temperature curves, different thermal analyses have been performed where all parts exposed to fire were given the same thickness. Longitudinal position is not relevant in this case anymore. The results are given in figure 12.2a for the lateral distance of 2.1 meter and in figure 12.2b for the lateral distance of 3.2 meter.

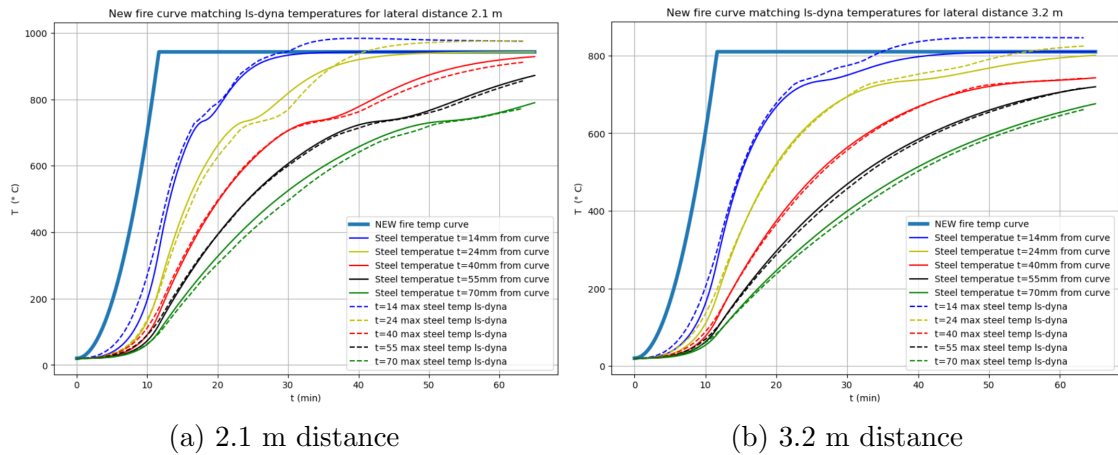


Figure 12.2: Adjusted temperature curve that result in steel temperature matching those from detailed LS-DYNA

The maximum temperatures of the newly created curves are 943 and 810 °C for the 2.1 and 3.2 m lateral distance respectively. It can be seen that there is a close match between the newly observed resulting steel temperatures from the adjusted temperature curves and the maximum temperatures obtained from detailed LS-DYNA analysis.

When applying these new temperatures with the reduced curve for the 2.1 m distance case on the model, the resulting time to reach plastic failure is 25 minutes (Both the wind and traffic leading load combination have been checked here). This is 10 minutes longer than the time to reach failure based on the HC fire curve. However, the critical time in the detailed analysis is 30 minutes, so there is still a 5-minute difference there. This means that both the fire scenario definition and the specification of the fire location plays an important role in the difference in result. In this new comparison, the fire scenario can be regarded as the same, and the lateral distance is taken into account, which led to the 10-minute resistance increase. But applying the temperatures as uniform still results in lower failure times than the performance based analysis, showing the conservatism's of the Eurocode methods. The same holds for the reduced temperature for 3.2-meter distance. Failure is reached there after 34 minutes, which is sufficiently long, but in the detailed analysis, plastic failure is not reached at all in the 63 minutes of analysis.

12.2 Cost and time effectiveness

Using the critical temperature limit of 350 °C provided by Eurocode is very fast. However, this results in high amounts of protection needed, which results in high costs, materials and carbon emissions. Applying protection on all arch sections up to portal height will cost 100k euro on intumescent paint (approximate value) only. Labor costs and other costs as a result of closing lanes are not yet taken into account here.

An intermediate approach where Eurocode steel temperatures are applied in the model requires a full model of the bridge. This takes quite some time and cost on the modeling side. The temperatures are based on the hydrocarbon fire curve, this considers the worst case fire scenarios. Uniform temperatures that depend on the section thicknesses are applied everywhere, which means exact fire position does not need to be considered. The total intumescent protection volume for each ASP with this calculation method is 4.1 times less than what was calculated based on the 350 °C limit. Taking this 350 °C is thus very conservative and is not recommended for economical design.

Modeling the detailed realistic fire scenarios requires even more time and cost on the modeling side. The extra steps taken here are the CFD run and investigations into which fire scenarios can be critical. However, this research has gained some useful insight that could speed up that process in possible future works and reduce the time and costs for these extra steps. The extra steps that need to be taken compared to applying uniform temperatures may very well be worth the cost it can save on fire protection measures.

Automation of the process is a big step in making the performance based analysis more time efficient. During this project, an automation script is already made that runs the thermal analysis, and then automatically uses the results of this thermal analysis as input for the GMNIA analysis and then runs the GMNIA analysis. This automation already made the process simpler and faster, even though obtaining the convection and radiation boundary conditions and obtaining the buckling modes were still done manually. Ideally, the automation would be expanded such that all the steps are taken given a model of the bridge (or 2 models, one thermal-only and one structural model) and fire specifications. These fire specifications include: Heat release, fire growth rate, longitudinal truck position, lateral distance from truck to bridge (and optionally: truck length).

The automation tool would then:

1. Write an FDS script based on the fire specification input, with data points

for convection and radiation at locations based on the bridge location and geometry.

2. Run the FDS file
3. Use the FDS results to obtain radiation and convection boundary conditions on the model and use these as input for the thermal analysis
4. Optional: run a linear buckling analysis (needs one more extra model as input) and take the buckling mode that occurs at the fire location as imperfection.
5. Run the thermal analysis
6. Use thermal results as input for the GMNIA analysis
7. Run GMNIA analysis

With a script that follows a workflow like this. Other bridges and fire scenarios could be addressed as well. This would make it a viable tool for real project design. The script that is already created only takes care of step 5 up to 7, expanding this workflow to include the other steps is something Arup would possibly be able to develop further.

13 Conclusion

The main research question in this report is: To which extent can detailed modeling of realistic fire scenarios applied on a case study of a 300-meter span steel arch bridge, bring savings in material use (and carbon emissions) in fire-resistant bridge design, and how can this detailed modeling be made cost and time efficient to be a viable tool for real project design.

This research shows that doing a detailed thermal structural analysis of fire on a steel bridge can indeed lead to material savings. Since the detailed performance based analyses show that the bridge does not fail in every considered fire scenario for at least 30 minutes, which is the required resistance time for this case study. When applying temperatures based on Eurocode curves, failure is reached after 15 minutes. The Eurocode method thus results in the conclusion that fire protection is necessary on the bridge, while the performance based analysis shows that it is not.

The total amount of protection with steel temperatures based on Eurocode curves applied on the model results in 4.1 times less protection volume for the arch than what is calculated based on the 350 °C limit that may be taken as critical temperature by Eurocode. Taking this 350 °C is thus very conservative and is not recommended for economical design.

The main reasons for the difference in results of code based methods and performance based models are, firstly, a higher fire load curve applied. Codes have limited options for fire curves and do not have the possibility to specify a realistic design fire scenario. The second reason is that uniform temperatures are applied on the sections with codified methods, not considering exact fire locations and view factors, whereas the performance based method does take those factors into account. Taking the limit of 350 °C does not take any project specific information or properties into account.

Some analysis on hanger loss has been done, the conclusion from the analysis is that the cables of the bridge cannot be left unprotected. However, there is still much potential to consider fire around the cables in more detail, which might result in a different conclusion.

Adjusted fire temperature curves can be created based on the fire growth input and the distance from burner to the bridge, the steel temperatures resulting from these adjusted curves match well with the maximum temperatures from the performance based analysis. An overview of the different failure times for the different

analyses based on these new curves is shown in figure 13.1

Fire model	Failure time (min)
Eurocode HC curve	15
Adjusted curve 2.1 m	25
Adjusted curve 3.2 m	34
Detailed analysis 2.1 m	30
Detailed analysis 3.2 m	>63

Figure 13.1: Failure times for different analysis

This research resulted in many conclusions regarding the importance of parameters influencing the problem. These can already help speed up the process would it be repeated on other projects. However, the remaining steps in the analysis still require much time. To really make the performance based modeling a viable tool for real project design, a workflow tool needs to be developed that automates and fastens the process. In this research, parts of the analysis steps were already automated, expanding this workflow to include other steps is something Arup would possibly be able to develop further.

14 Discussion

Three different methods have been compared. The first method was a calculation in temperature domain. No forces were taken into account in this method. The number of 350 °C is based on the fact that almost no strength reduction is happening in the steel at that temperature. The 350 degree limit does thus not take the utilization state of the members into account, not taking this into account is the reason this method is very conservative, this was also concluded from the resulting protection necessary. Furthermore, this method does not result in any insight in the behavior of the bridge under fire loading.

In the second method, where temperatures from curves are applied uniformly on the model, both a time domain and temperature domain calculation have been done. The time domain calculation result in a failure time given a certain fire scenario and the temperature domain calculation resulted in a critical temperature value, for a specified resistance time of 30 minutes. This critical temperature is 600 °C. This method gives proper critical temperature values that can be used for design, since it takes geometry, material properties and loads into account. Failure times are however not representative for reality, since the uniformly applied temperatures does not represent reality and therefor the failure modes and times will also differ.

For the third method, which is the detailed performance based analysis, results are presented in time domain. Failure times are computed given a certain design fire scenario. These failure times are representative of reality, since all fire dynamics and specifications are taken into account, this method is therefore the only method that gives insight into the actual behavior of the bridge under fire loading.

There is one more domain in which the capacity of the bridge can be calculated, which has not been done in this research. This is the force domain, where the results are presented as a factor with which the loads could be multiplied to reach failure after a defined time and fire scenario, this can be done in an iterative process where the loads should be adjusted until the exact required failure time is reached, or by keeping the temperature constant after the required resistance time is reached, and then ramping up the loads until failure is reached. This is something that could be done in further research or work on this project.

There are still some limitations to this research. The most important one is the bridge geometry that is not modeled in the CFD analysis, meaning fire-structure interaction is not considered. This is a something that is interesting for further research. Another limitation is that the members in the model that are exposed

to elevated temperatures are chosen. This choice is based on the assumption that flanges and webs not facing the fire will not receive radiation, and therefore the temperature rise is negligible. And that elements outside a certain distance of the fire will not be affected. This choice can be made differently and will likely have effect on the quantitative results.

Furthermore, the influence of other variables that were constant in this research would be interesting to investigate. These are: The maximum heat release rate of the fire and the increasing modulus, which is how fast the fire grows and reaches its maximum. In this research, these values are taken as fixed. One example might be a fire with a HRR curve that matches the shape of the hydrocarbon fire curve.

Another interesting follow-up research would be if the differences in capacity and necessary protection that result from this research are similar for longer fire durations. And for this case study specific, it would be interesting to do a more detailed investigation in fire scenarios around the hangers.

References

- [1] J. Alos-Moya et al. “Analysis of a bridge failure due to fire using computational fluid dynamics and finite element models”. In: *Engineering Structures* 68 (2014), pp. 96–110. ISSN: 0141-0296. DOI: <https://doi.org/10.1016/j.engstruct.2014.02.022>. URL: <https://www.sciencedirect.com/science/article/pii/S0141029614001151>.
- [2] Esam M. Aziz et al. “Behavior of steel bridge girders under fire conditions”. In: *Journal of Constructional Steel Research* 106 (2015), pp. 11–22. ISSN: 0143-974X. DOI: <https://doi.org/10.1016/j.jcsr.2014.12.001>. URL: <https://www.sciencedirect.com/science/article/pii/S0143974X14003253>.
- [3] Burak Kaan Cirpici, Y.C. Wang, and B. Rogers. “Assessment of the thermal conductivity of intumescent coatings in fire”. In: *Fire Safety Journal* 81 (2016), pp. 74–84. ISSN: 0379-7112. DOI: <https://doi.org/10.1016/j.firesaf.2016.01.011>. URL: <https://www.sciencedirect.com/science/article/pii/S0379711216300133>.
- [4] Carlos Couto et al. “Numerical validation of the general method for structural fire design of web-tapered beams”. In: *Eurosteel 2014*. 2014.
- [5] Ashraf ElSabbagh et al. “Inelastic buckling analysis of steel columns at different fire scenarios”. In: *Engineering Structures* 291 (2023), p. 116464. ISSN: 0141-0296. DOI: <https://doi.org/10.1016/j.engstruct.2023.116464>. URL: <https://www.sciencedirect.com/science/article/pii/S0141029623008799>.
- [6] Jiayu Hu, Ricky Carvel, and Asif Usmani. “Bridge fires in the 21st century: A literature review”. In: *Fire Safety Journal* 126 (2021), p. 103487. ISSN: 0379-7112. DOI: <https://doi.org/10.1016/j.firesaf.2021.103487>. URL: <https://www.sciencedirect.com/science/article/pii/S0379711221002290>.
- [7] Rahul Kallada Janardhan et al. “Coupled CFD-FE analysis of a long-span truss beam exposed to spreading fires”. In: *Engineering Structures* 259 (2022), p. 114150. ISSN: 0141-0296. DOI: <https://doi.org/10.1016/j.engstruct.2022.114150>. URL: <https://www.sciencedirect.com/science/article/pii/S014102962200284X>.
- [8] Mustesin Ali Khan et al. “Fire hazard assessment, performance evaluation, and fire resistance enhancement of bridges”. In: *Structures* 34 (2021), pp. 4704–4714. ISSN: 2352-0124. DOI: <https://doi.org/10.1016/j.structures.2021.103487>.

- istruc.2021.10.080. URL: <https://www.sciencedirect.com/science/article/pii/S2352012421010407>.
- [9] V.K.R. Kodur and M.Z. Naser. “Effect of shear on fire response of steel beams”. In: *Journal of Constructional Steel Research* 97 (2014), pp. 48–58. ISSN: 0143-974X. DOI: <https://doi.org/10.1016/j.jcsr.2014.01.018>. URL: <https://www.sciencedirect.com/science/article/pii/S0143974X14000406>.
- [10] V.K.R. Kodur and M.Z. Naser. “Effect of local instability on capacity of steel beams exposed to fire”. In: *Journal of Constructional Steel Research* 111 (2015), pp. 31–42. ISSN: 0143-974X. DOI: <https://doi.org/10.1016/j.jcsr.2015.03.015>. URL: <https://www.sciencedirect.com/science/article/pii/S0143974X15000991>.
- [11] V.K.R. Kodur and M.Z. Naser. “Designing steel bridges for fire safety”. In: *Journal of Constructional Steel Research* 156 (2019), pp. 46–53. ISSN: 0143-974X. DOI: <https://doi.org/10.1016/j.jcsr.2019.01.020>. URL: <https://www.sciencedirect.com/science/article/pii/S0143974X18305066>.
- [12] Zhi Liu, Guo-Qiang Li, and Yuan Ren. “Performance of steel cable-stayed bridges in ship fires, Part II: Influencing factors and mechanisms”. In: *Journal of Constructional Steel Research* 211 (2023), p. 108057. ISSN: 0143-974X. DOI: <https://doi.org/10.1016/j.jcsr.2023.108057>. URL: <https://www.sciencedirect.com/science/article/pii/S0143974X23002845>.
- [13] Rujin Ma et al. “Performance-based design of bridge structures under vehicle-induced fire accidents: Basic framework and a case study”. In: *Engineering Structures* 197 (2019), p. 109390. ISSN: 0141-0296. DOI: <https://doi.org/10.1016/j.engstruct.2019.109390>.
- [14] Élio Maia et al. “The General Method for the fire design of slender I-section web-tapered columns”. In: *Thin-Walled Structures* 155 (2020), p. 106920. ISSN: 0263-8231. DOI: <https://doi.org/10.1016/j.tws.2020.106920>. URL: <https://www.sciencedirect.com/science/article/pii/S0263823120307989>.
- [15] Isidoro Martínez. *Radiative view factors*. 1995. URL: <http://imartinez.etsiae.upm.es/~isidoro/tc3/Radiation%20View%20factors.pdf>.
- [16] M.Z. Naser and V.K.R. Kodur. “Comparative fire behavior of composite girders under flexural and shear loading”. In: *Thin-Walled Structures* 116 (2017), pp. 82–90. ISSN: 0263-8231. DOI: <https://doi.org/10.1016/j.tws.2017.03.003>. URL: <https://www.sciencedirect.com/science/article/pii/S0263823117302537>.

- [17] Samer Nemer, József A. Szalai, and Ferenc Papp. “The overall imperfection method for fire design situation”. In: *Engineering Structures* 283 (2023), p. 115884. ISSN: 0141-0296. DOI: <https://doi.org/10.1016/j.engstruct.2023.115884>. URL: <https://www.sciencedirect.com/science/article/pii/S0141029623002985>.
- [18] *NEN-EN 1990*. 2019.
- [19] *NEN-EN 1990+A1+A1/C2/NB*. 2019.
- [20] *NEN-EN 1991-1-2+C3*. 2019.
- [21] *NEN-EN 1993-1-1*. 2016.
- [22] *NEN-EN 1993-1-11/NB*. 2009.
- [23] *NEN-EN 1993-1-5*. 2012.
- [24] I. Payá-Zaforteza and M.E.M. Garlock. “A numerical investigation on the fire response of a steel girder bridge”. In: *Journal of Constructional Steel Research* 75 (2012), pp. 93–103. ISSN: 0143-974X. DOI: <https://doi.org/10.1016/j.jcsr.2012.03.012>. URL: <https://www.sciencedirect.com/science/article/pii/S0143974X12000661>.
- [25] G. Peris-Sayol et al. “Analysis of the influence of geometric, modeling and environmental parameters on the fire response of steel bridges subjected to realistic fire scenarios”. In: *Computers Structures* 158 (2015), pp. 333–345. ISSN: 0045-7949. DOI: <https://doi.org/10.1016/j.compstruc.2015.06.003>. URL: <https://www.sciencedirect.com/science/article/pii/S0045794915001923>.
- [26] *prEN 1993-1-14*. 2023.
- [27] Jinggang Zhou et al. “Numerical study of the convective heat transfer coefficient for steel column surrounded by localized fires”. In: *Fire Safety Journal* 141 (2023), p. 103987. ISSN: 0379-7112. DOI: <https://doi.org/10.1016/j.firesaf.2023.103987>. URL: <https://www.sciencedirect.com/science/article/pii/S0379711223002552>.
- [28] Jinggang Zhou et al. “Comparison of different CFD-FEM coupling methods in advanced structural fire analysis”. In: *International Journal of Thermal Sciences* 193 (2023), p. 108465. ISSN: 1290-0729. DOI: <https://doi.org/10.1016/j.ijthermalsci.2023.108465>. URL: <https://www.sciencedirect.com/science/article/pii/S1290072923003265>.

- [29] Qiling Zou, Kavi Pool, and Suren Chen. “Performance of suspension bridge hangers exposed to hazardous material fires considering wind effects”. In: *Advances in Bridge Engineering* 1 (2020). ISSN: 2662-5407. DOI: 10.1186/s43251-020-00004-9.

Appendix A: Stakeholders and societal impact

The main stakeholders that are relevant to this research are:

- The bridge owner (Client of the company)
- Users of the bridge
- The project consultant (Company)
- Research community
- Bridge engineering industry

The client, which is the bridge owner, is also the main stakeholder in this case study.

The main needs and wishes for the client are that the bridge is safe. Since the design of the bridge is complete, the safety is not in question. But a second important need/wish for the client is that the amount of money needed for protection/renovation/assessment is minimized, while being more confident in the bridge its performance. It is therefore interesting for the client to see what the result of this research will be. The project consultant has in this regard the same values as the bridge owner. These values are also the main reason to research this topic.

The main value for the users of the bridge is first and most important of all, the safety of the bridge. A second value that can be important for drivers is the bridge's aesthetics. They do not have any responsibility regarding the design or maintenance of the bridge, only in driving safely over it. For the research community, new insights are the most important value that result from this research, they are responsible for the development of science and knowledge and this research can bring new insights in the realistic behavior of existing bridges under fire loading. These same values as for the research community are also true for the bridge engineering industry, except that their responsibility is to apply the gained knowledge to safely design or assess bridges.

This research will result in greater understanding into the performance of steel bridges under fire conditions and in a demonstrated potential reduction in the necessary fire protection measures, this would have significant benefits. of which the most important are:

- Reduced cost
- Reduced material use (and associated embodied carbon cost)

- Increased confidence in performance
- Reduced impact on aesthetics and architectural expression

These benefits would not only be relevant for the bridge in the case study considered, but also for future new bridge design and for the maintenance and renovation of the vast network of existing steel bridges globally, many of which are approaching the end of their original design life.

It can be seen from the values and responsibilities mentioned for each stakeholder above, and the benefits that result from this research, that all stakeholder can be positively impacted by the results.

Appendix B: Thermal material properties

All thermal material properties are taken from NEN-EN 1993-1-2 For the whole bridge, steel grade S355 is used. For the yield stress and Young's modulus, tabulated reduction factors are used on the initial values. Figure B.1 shows the reduction factors as a function of temperature in a graph. These are valid for section in cross-section class 4.

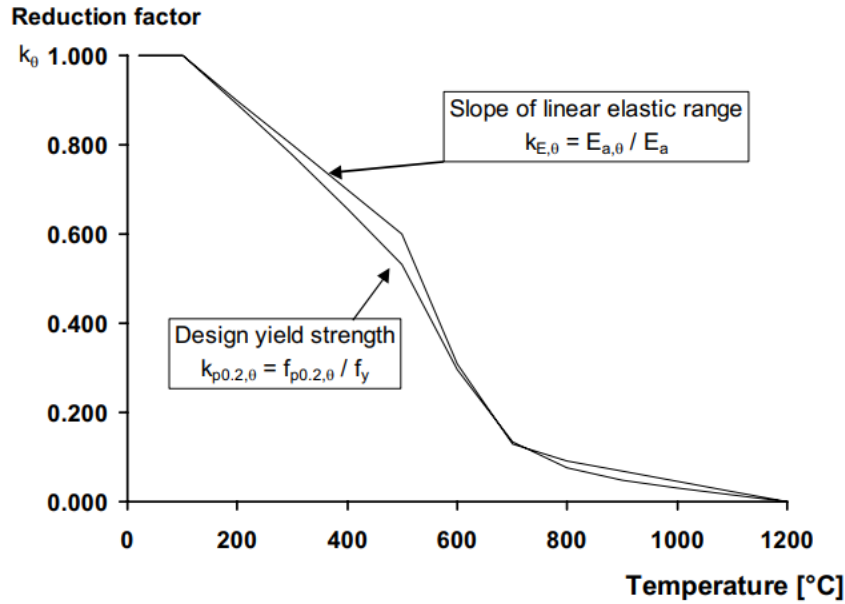


Figure B.1: Reduction factors Youngs modulus and yield stress

For the specific heat, the following temperature dependent values are used

For $20 \text{ }^{\circ}\text{C} \leq \theta_a < 600 \text{ }^{\circ}\text{C}$

$$c_a = 425 + 7.73 \cdot 10^{-1} \theta_a - 1.69 \cdot 10^{-3} \theta_a^2 + 2.22 \cdot 10^{-6} \theta_a^3$$

For $600 \text{ }^{\circ}\text{C} \leq \theta_a < 735 \text{ }^{\circ}\text{C}$

$$c_a = 666 + \frac{13002}{738 - \theta_a}$$

For $735 \text{ }^{\circ}\text{C} \leq \theta_a < 900 \text{ }^{\circ}\text{C}$

$$c_a = 545 + \frac{17820}{\theta_a - 731}$$

For $900 \text{ }^{\circ}\text{C} \leq \theta_a < 1200 \text{ }^{\circ}\text{C}$

$$c_a = 650$$

Figure B.2 shows the specific heat as a function of temperature.

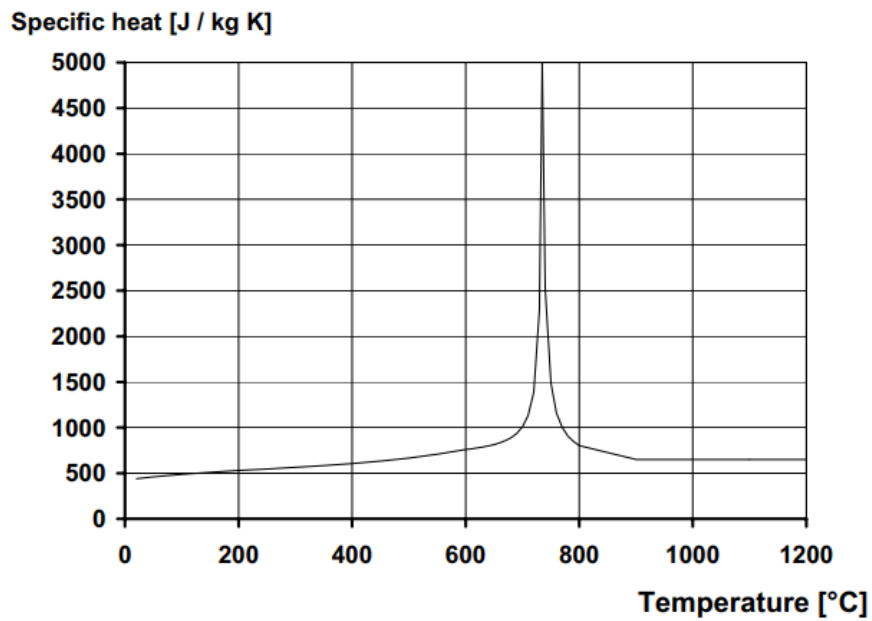


Figure B.2: Specific heat as a function of temperature

The thermal conductivity of steel λ_a is defined as follows:

$$\begin{aligned} &\text{For } 20 \text{ } ^\circ\text{C} \leq \theta_a < 800 \text{ } ^\circ\text{C} \\ &\lambda_a = 54 - 3.33 \cdot 10^{-2} \theta_a \\ &\text{For } 800 \text{ } ^\circ\text{C} \leq \theta_a < 1200 \text{ } ^\circ\text{C} \\ &\lambda_a = 27.3 \end{aligned}$$

Figure B.3 shows the thermal conductivity as a function of temperature.

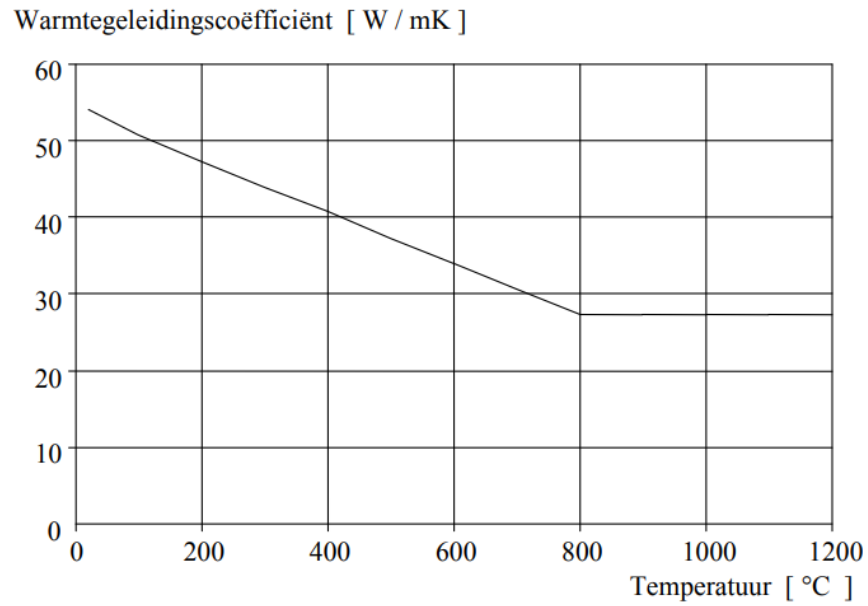


Figure B.3: Thermal conductivity as a function of temperature

And the thermal expansion coefficient α_a

For $20\text{ }^{\circ}\text{C} \leq \theta_a < 750\text{ }^{\circ}\text{C}$

$$\alpha_a = 1.2 \cdot 10^{-5} + 0.4 \cdot 10^{-8} \theta_a$$

For $750\text{ }^{\circ}\text{C} \leq \theta_a < 860\text{ }^{\circ}\text{C}$

$$\alpha_a = 0$$

For $860\text{ }^{\circ}\text{C} \leq \theta_a < 1200\text{ }^{\circ}\text{C}$

$$\alpha_a = 2 \cdot 10^{-5}$$

Appendix C: Test model

A test model has been used where all steps in the analysis are taken to validate the results and to see if everything works as it should. The test model can be seen in figure C.1. This test model is a simple representation of the portal frame of the bridge, so the sides of this frame represents the arch. This model consist of beam and shell elements. The shell elements are used at locations close to the fire, that is where the model should be the most detailed.

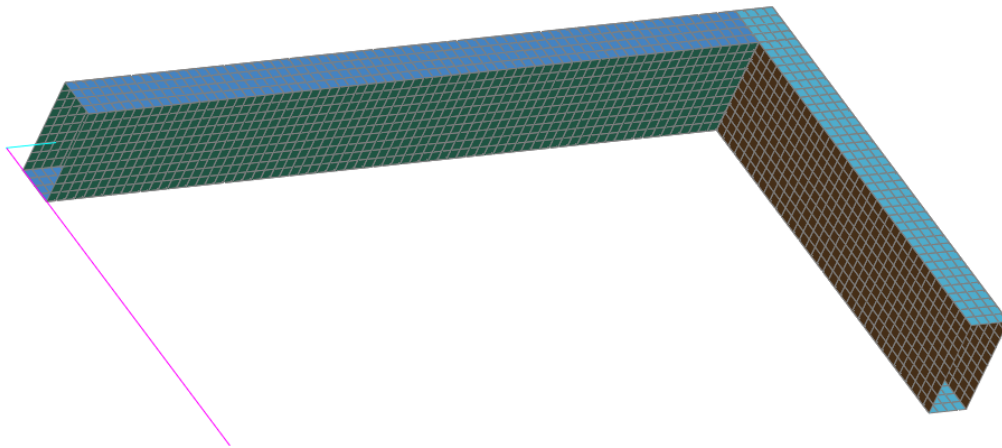


Figure C.1: Test model

The steps that need to be taken are:

- Get radiation and convection boundary conditions from the CFD results
- Get the steel temperature vs time (Thermal analysis)
- Do a linear buckling analysis to obtain buckling modes (Buckling analysis)
- Get nodes for model with imperfections
- Do a full GMNIA analysis with the steel temperature from the thermal analysis and the imperfection nodes obtained with the buckling analysis as input

C.1 Thermal analysis

For the thermal analysis, CFD result were used from one of the 4 simulation, this was the open truck fire with 3m/s wind.

The location of the bridge fire could be modelled by moving the bridge w.r.t. location of the data points of the CFD. The arch is between the CFD data points, and the fire is located over a length of 16 meters just below the portal as shown in figure C.2

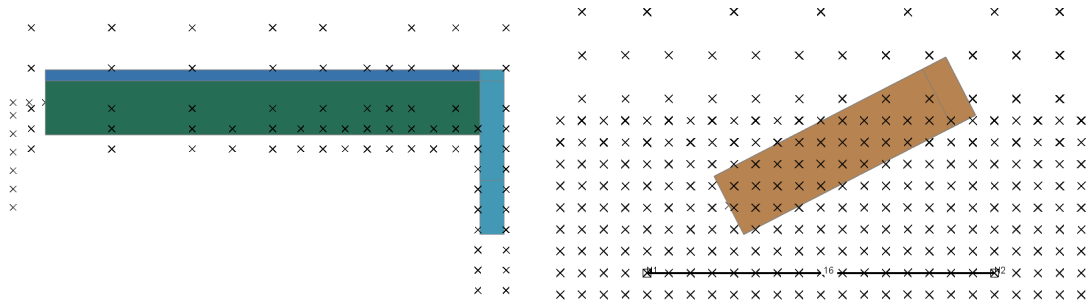


Figure C.2: CFD data points location w.r.t. the test model

With an already existing JavaScript, the boundary convection and boundary radiation input files could be generated bases on the location of the bridge and the CFD results. With this convection and radiation again used as input, the thermal analysis could be run.

The resulting temperature from this thermal analysis can be seen in figure C.3

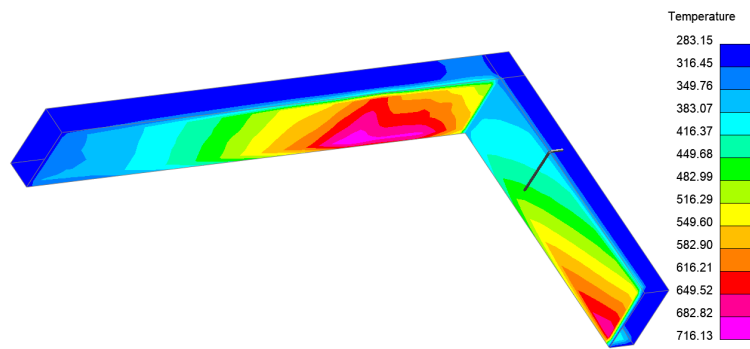


Figure C.3: Test model temperatures

C.2 Buckling analysis

The goal of the buckling analysis is to obtain the buckling mode shapes, such that that shape can be used as the shape of the imperfection. For this, an implicit eigenvalue analysis has been done. the amount of modes to be calculated by the

analysis has been set to 100. The critical buckling mode that will be used for the nodes of the imperfections, are the buckling modes which are located at the location where the steel is most affected by the fire, and then the one with the lowest load factor.

The resulting nodes of the imperfections have been checked with a quick manual calculation. For this calculation, the node ID of the node with the maximum displacement was obtained from the buckling analysis. For this node, the node coordinates of the original structure were taken. Then the displacement of this node due to static loads was determined. The coordinates of the node when statically displaced are then known. These are compared to the nodes of the model with imperfections. The size of the imperfection is calculated according to NEN-EN 1993-1-5 and is in this case 15 mm or 0.015 m

A limitation to this analysis is that the thermal loads are not yet taken into account. For that reason, the same analysis has been done but with thermally reduced material properties. To do this, the following steps were taken.

1. The temperature of each element has been extracted from the thermal analysis results after a fire duration of 30 minutes.
2. The reduced yield strength and E modulus have been calculated for each of these elements. Based on the extracted temperatures.
3. Each element was recreated in the finite element model with a new part that has the new reduced material properties.

This analysis takes more time to model, and is more computationally expensive. However, with this approach, the location of the fire is taken into account in the buckling mode, so taking the buckling mode with the lowest load factor will be the critical buckling mode. This way, only 1 buckling mode for each fire and load combination has to be checked.

For both of the buckling analysis types, the resulting first buckling mode can be seen in figure C.4. The left figure is without thermally reduced material properties, the right one with. The second and third buckling mode are also shown in figure C.5 and C.6.

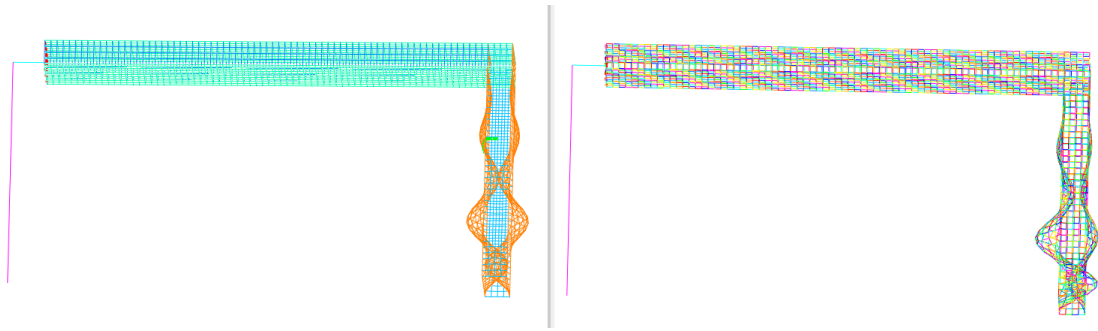


Figure C.4: Buckling mode 1

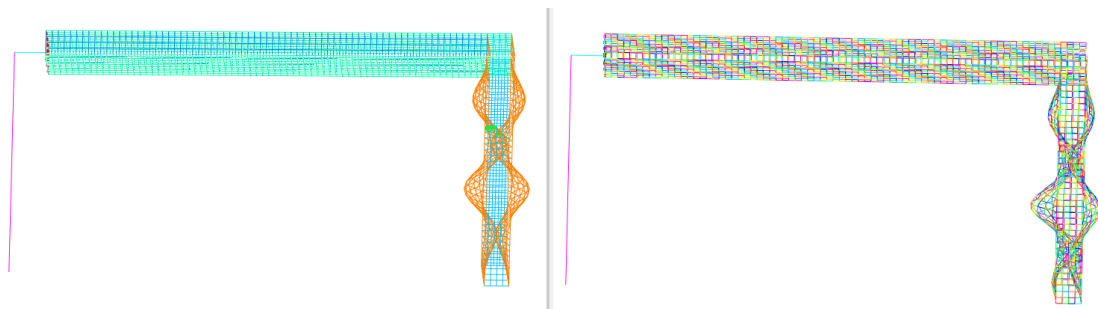


Figure C.5: Buckling mode 2

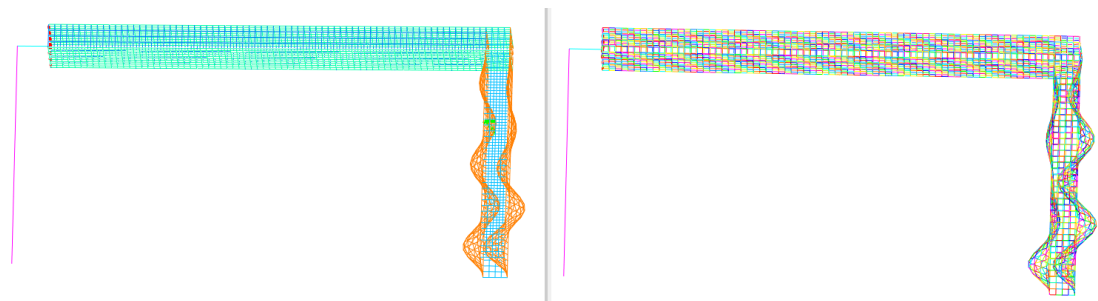


Figure C.6: Buckling mode 3

It can be seen that the location of the buckled parts of the buckling modes is similar. This is also the case for the even higher buckling modes. The maximum imperfections are the same for both cases, since this is scaled to the value from Eurocode. So there is no significant difference between the two types of buckling analysis. This means that in the rest of the research, the simplest of these two is used, which is the linear buckling analysis without reduced material properties.

C.3 GMNIA analysis

With the new model nodes with imperfections included, obtained from the buckling analysis, and the temperatures from the thermal analysis as thermal load input, a full GMNIA analysis was done. Figure C.7 shows the plastic strain after 30 minutes of fire. It can be seen that the locations of high plastic strain are concentrated at the locations where the highest temperatures occur.

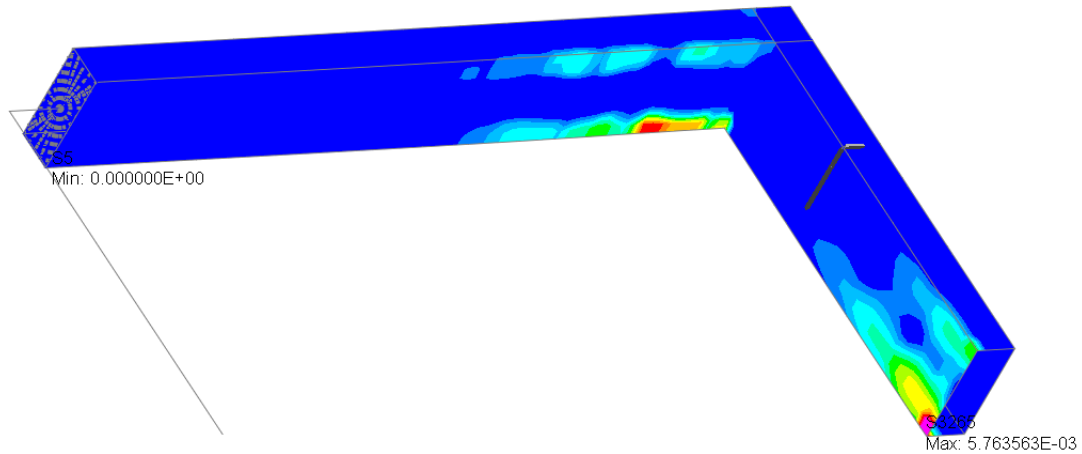


Figure C.7: Plastic strain of GMNIA analysis test model

The results of the test model are as expected, so the methods that are used in the FEM models will be used in the full bridge model as well.

Appendix D: Arch and main girder UC calculations

This appendix show the unity checks for the arch and main girder that were done for the hanger loss scenarios.

In the calculations of the arch, the stiffeners are not taken into account when checking plate buckling of the webs. This is a conservative assumption, since the stiffeners increase the critical buckling load. The stiffeners are taken into account for the area and inertia calculations.

The effective area reduction factors and effective width on both ends of a plate were calculated with an internal calculation tool at Arup that needs the plate dimensions, corner stresses (stresses at the plate ends) and yield stress as input.

As can be seen from the Unity Checks, the arch is able to resist the loads in the hanger loss cases. The main girder is not.

Appendix E: Cross-section class calculation

The critical temperatures determined with Eurocode is dependent on the cross-section class. Therefore, the cross-section class of the arch section is calculated here. The first section of the arch at the location of the arch springing point (ASP) has the following cross-section properties.

- Web thickness: 55 mm
- Web height: 3642 mm
- Flange thickness: 70 mm
- Flange width: 1310 mm

For the flange, this results in:

$$c/t = (1310 - 2 \cdot 55)/70 = 1200/70 = 17.14$$

And for the web:

$$c/t = (3642 - 2 \cdot 70)/55 = 3502/55 = 63.67$$

In the case of fire, cross-sections can be classified the same way as for normal temperatures with a reduced value of 0.85 as shown in, which takes into account the influence of the temperature increase, the value for ϵ to classify cross-section can be calculated with equation 25 which is from Eurocode 1993-1-2 section 4.2.

$$\epsilon = 0.85 [235/f_y]^{0.5} \quad (24)$$

With steel grade S355 and an element thickness > 40 mm, $f_y = 335 \text{ N/mm}^2$, this results in $\epsilon = 0.71$. From design calculations for normal circumstances, it was seen that the cross-section is fully in compression. Combining bending and compression with no tension in the cross-section, so with $\psi = 0$ according to table 5.2 from NEN-EN 1993-1-1 [21] will result in a CSC 3 limit of:

$$c/t < \frac{42\epsilon}{0.67 + 0.33\psi} = 44.6 \quad (25)$$

This means the section is in CSC 4.

Appendix F: GMNIA results for different imperfections

Some small tests have been done to see the effect of different imperfections at different locations. The resulting plastic strain and the von Mises stress after 30 minutes of fire (at $t = 3.8$ s in this analysis) can be seen in figures F.1 up to F.3.

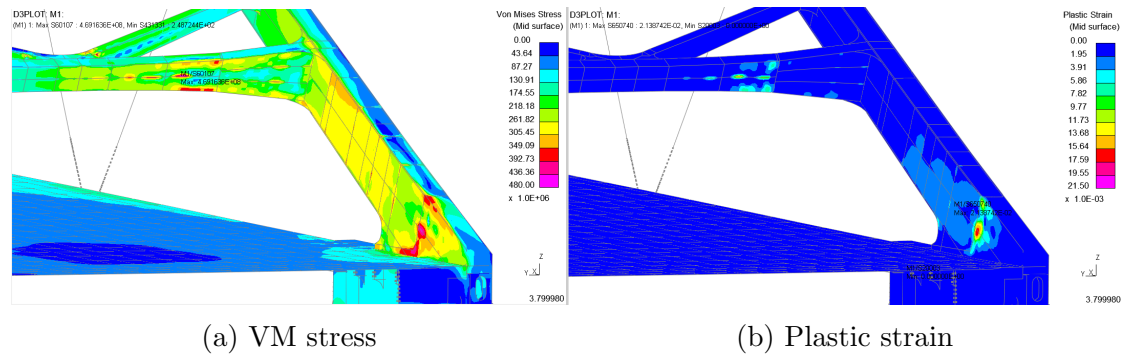


Figure F.1: No imperfections used

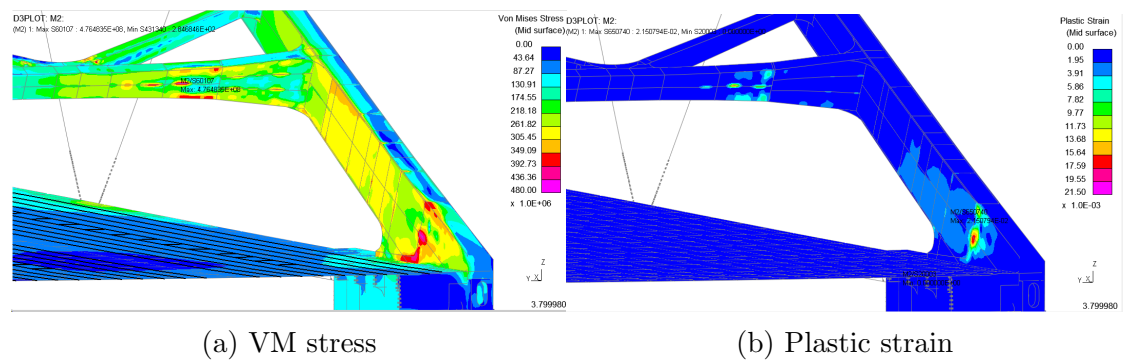


Figure F.2: Imperfection 1

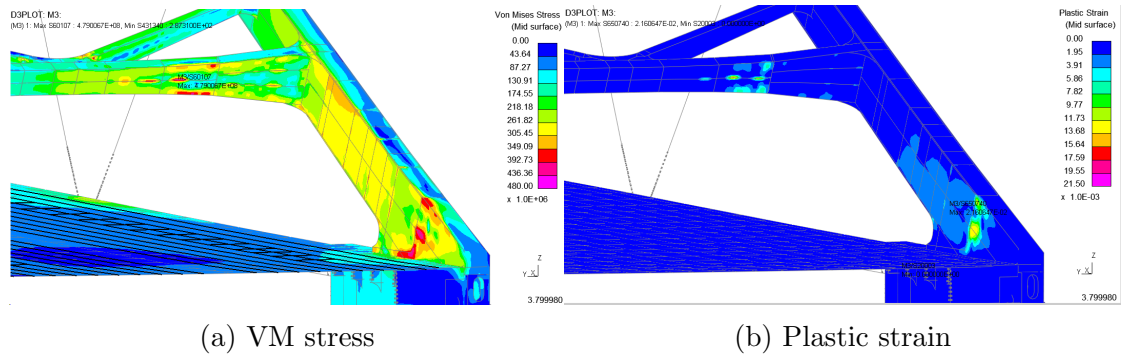


Figure F.3: Imperfection 2

It can be seen in the figures that for location and magnitudes of the stresses and strains and the maxima are almost identical. This is also the case at other times which are not presented here. This means that modeling imperfections in general has very little effect on the outcome, and so does the location of the imperfections. A limitation to this sub-study is that this analysis has been done for one location, fire scenario and load combination. But the buckling modes are clearly within the affected area, so other fire scenario's and load combinations are expected to give the same result.

Appendix G: Increased steel thickness as protection

Increasing the thickness of the steel members subjected to fire can lead to an increase in fire resistance. There are two reasons for this. Firstly, increasing the thickness results in lower temperatures of the member. This is because the section factor reduces. Secondly, there is an increase in capacity of the member when the thickness is increased.

For the Eurocode thermal load. All sections located around the fire have to be increased in thickness. If only one section of the arch is increased, failure will develop in another thinner section next to it. A GMNIA analysis has been performed with sections of the arch up to portal height with a thickness of 70 mm. This increased the failure time from 15 minutes to 29 minutes. This is almost double the resistance time, but it is still not the required 30 min. Furthermore, the amount of extra steel required relative to the original thicknesses is quite significant, with up to 75% thickness increases.

For the GMNIA of the most critical fire scenario, which reached the failure strain after 30 minutes, the effect of increasing steel thickness has been investigated as well. For the performance based model, only few sections need to be adjusted in thickness, since the effect of the fire is local as well. For the most critical fire scenario, the sections with a thickness of 40 mm at the arch springing point, shown in green in figure G.1, have been increased to 55 mm.

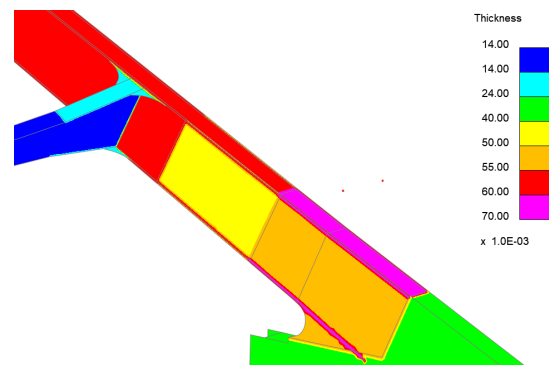


Figure G.1: Section thicknesses at the arch springing point

By increasing this thickness, the plastic failure strain limit was not reached until the end of the analysis, which means at least more than 63 minutes before plastic failure. A second run has been executed with the increased thickness in the thermal analysis only, but not in the GMNIA, meaning the temperature over time is different, but the capacity of the section is the same. In this scenario,

plastic failure was reached after 41 minutes. A third run was performed where the temperatures were based on the 40 mm plate, but a 55 mm plate was used in the GMNIA analysis. The failure time here was 37 min. This shows that the extra resistance time results from both the reduced temperatures and increased capacity, but with the temperature distribution having the most influence.

Using these increased plate thicknesses can be a cost-effective way to improve the fire resistance, since steel prices are relatively low compared to that of intumescent paints, and the whole process of applying and maintaining the paint can be avoided.